Feedback Volterra control of integro-differential equations

G. Pepe, E. Paifelman & A. Carcaterra

Published online: 29 Aug 2022.

Submit your article to this journal ☑

Article views: 14

View related articles ☑

View Crossmark data ☑

Feedback Volterra control of integro-differential equations

G. Pepe [a], E. Paifelman[b] and A. Carcaterra[a]

[a]Department of Mechanical and Aerospace Engineering, Sapienza, University of Rome La Sapienza, Rome, Italy; [b]Institute of Marine Engineering National Research Council, Rome, Italy

ABSTRACT
This paper describes a general physical background that originates integro-differential problems with specific reference to aero-elastic coupling, and offers two techniques of control for this class of problems. The central result of the paper is that integro-differential equations with kernel exponential series admit an optimal solution described, in turn, by a Volterra integral equation in terms of the control. Numerical simulations show how controls prevent the flutter instability of a two-dimensional wing and a wind turbine blade.

1. Introduction

Integro-differential equations (IDEs) (Kochetkov & Tomshin, 1978) form the mathematical basis of many physical applications which have been studied in recent years (Dehghan & Shakeri, 2008; Rao & Allison, 2015; Rezaei et al., 2019; Sachs & Strauss, 2008). These equations represent an open challenge for optimal control investigations (Abdel Hafeez & El-Badawy, 2018; Kumar et al., 2020; Mo et al., 2015; Vasconcellos et al., 2016; Wolf et al., 2015; Yang & Strganac, 2013).

The dynamics of an integro-differential model differ in a substantial way with respect to more standard simpler differential equations, introducing memory effects into the system's response, sometimes through the presence of convolution integrals. These memory effects appear when the system dynamic involves the interaction with the surrounding environment and describe the system's response in a more accurate form, that in some unfortunate conditions can be subject to dynamic instability.

Typically, these kinds of models are well represented by the integro-differential equations of Volterra type and the application of optimal control to them is still under investigation by several authors (Belbas, 2007, 2008; Benjamin et al., 2007; Tao & Gao, 2020; Vijayakumar, 2018; Vinokurov, 1969).

Normally, this implies the use of approximated methods of solution. In fact, nonlinear Volterra's problems use mainly direct methods. Through the discretization of the control problem, these methods make use of nonlinear dynamic programming, solved by standard large-scale optimisation algorithms (Maleknejad & Ebrahimzadeh, 2014). Some examples are formulated by (Belbas, 2008) and (Benjamin et al., 2007), which introduce iterative methods to obtain the optimal control of a nonlinear integral equation, under some conditions for the kernel of the integral equation. In (Marzban & Rostami Ashani, 2020) some hybrid numerical methods for solving the control problem of nonlinear Volterra integral equations are proposed.

Projection solution methods, based on orthogonal functions, have been utilised by (Maleknejad & Almasieh, 2011; Yan & Lu, 2016) with triangular functions for approximating control and state variables, and in (Tohidi & Samadi, 2013) the authors proposed the use of Lagrange basis functions in controlling nonlinear Volterra systems. Recently, in this context, wavelet functions attracted considerable attention among researchers (Singha & Nahak, 2018; Yousefi et al., 2011), which make use of the Legendre multi-wavelet collocation method for solving fractional optimal control problems. A new method for optimal control of Volterra integral equations can be found in (Belbas, 2007), where the authors utilise discretization of the original Volterra controlled system and a novel type of dynamic programming, in which the Hamilton–Jacobi function is parametrised by the control function. Moreover, the authors have recently proposed a different indirect variational method for IDEs. This contribution uses the variational theory of Pontryagin (Pepe & Carcaterra, 2014; Pepe et al., 2020; Pontryagin, 2018), normally applied to differential equations, to integro-differential models.

Three new elements emerge in this context: (i) the optimal solution is obtained by the direct application of the variational calculus to Volterra's equation, (ii) an open-loop implicit solution of the optimal control problem is obtained, and (iii) a feedback control formulation is proposed, through a model predictive control for IDEs (Paifelman, 2017; Paifelman et al., 2018; Paifelman et al., 2019, 2021; Pepe et al., 2021; Pepe et al., 2020a, 2020b).

In this general scenario, the present paper aims to propose a feedback-based control algorithm applied to Volterra integro-differential equations of the first species, useful to represent, in a simplified way, many physical models such as the wind turbine dynamics, aeroplane's wings flutter, bridges and suspended cables fluctuations, floating bodies and hydrodynamic lifting surfaces (de Andrade, 2018; Levinson, 1960; Newman, 1979; Sachs & Strauss, 2008; Solodusha, 2020).

The element of originality of the present method is that thanks to the use of Laplace transform, the problem of a minimum of the objective function is directly solved by a variational approach, even in the presence of Volterra integrals.

In Section 2, a common basis for the presence of convolution terms in the governing equations of a general category of physical systems is outlined. A prototype linear integro-differential equation is considered, introducing two different control methods (Section 3). The main conclusion is that a control obeying a Volterra-type integral equation represents the solution of the optimal control problem of the original integro-differential equation, provided that its kernel is decomposable as an exponential series.

Finally, the two control algorithms are compared for two typical engineering examples, investigated in detail in Section 4: the two-dimensional wing in an unsteady flow, and the wind turbine blade in which the control avoids the inception of unstable flutter phenomena.

2. A common physical background for integro-differential operators

A rather general physical mechanism, that generates integro-differential equations, comes when coupling two physical fields, as in the particular case of the fluid-structure coupling.

When the two coupled differential equations of the two fields are manipulated, so that one of the two fields' variable disappear (hidden variable), the remaining equation includes a convolution term, besides the differential ones.

Let us make a general and more detailed point about this physical background of integro-differential operators. Introduced originally by the authors in (Carcaterra et al., 2015), this argument is here refined and summarised.

Suppose we are interested in modelling and controlling a spatially confined linear system S surrounded by a second system E, the environment where, for example, S is the structure and E is the surrounding fluid (see Figure 1). Assume the field variable $\Phi(x, t)$ describes S, in general dependent on both space x and time t, through the differential equation $L_\Phi\{\Phi\} = f_{E \to S}(\Phi, \Psi)$, where L_Φ is in general a linear partial differential operator. $f_{E \to S}$ represents the interaction between S and E, i.e. the forces applied by E to S. $f_{E \to S}$ depends on both Φ and Ψ, since it is an interaction force, and E is described by the field variable $\Psi(x, t)$. Moreover, $L_\Psi\{\Psi\} = f_{S \to E}(\Psi, \Phi)$ is the equation of evolution of the environment E, and $f_{S \to E} = -f_{E \to S}$, because of the action-reaction principle, is the force applied by the system to the environment, through the common boundary $\partial S \equiv \partial E$ between S and E.

If under the hypothesis of linearity, we assume $f_{S \to E} = A_\Psi \Psi + A_\Phi \Phi$, then $L_\Psi\{\Psi\} - A_\Psi \Psi = A_\Phi \Phi$.

The formal solution to this last equation can be obtained considering $A_\Phi \Phi$ as a known term, forcing the equation of the field Ψ. The method of the Green function (Byron & Fuller, 2012), permits to express the solution of the equation $L_\Psi\{\Psi\} - A_\Psi \Psi = A_\Phi \Phi$. In fact, considering the Green function G of the operator $L_\Psi\{\cdot\} - A_\Psi \cdot$, one obtains the form:
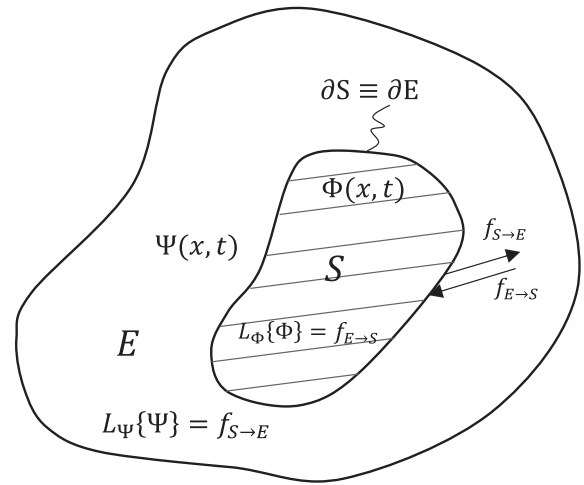
$$\Psi = A_\Phi G * \Phi \qquad (1)$$

Figure 1. Illustration of the interaction between the S and E.

This expression is substituted into the equation of evolution of S, obtaining:

$$L_\Phi\{\Phi\} + A_\Phi \Phi + A_\Psi A_\Phi G * \Phi = 0 \qquad (2)$$

In Equation (2), the field variable Ψ of E does not appear anymore. The effect of the interaction between S and E can now be expressed only by using the variable Φ of S, through the integral term $A_\Psi A_\Phi G * \Phi$. We call Ψ the hidden variable. This procedure, even if in many cases is not explicit in a clear and conscious way, is common to many physical problems leading to integro-differential equations. And this is also the physical basis of the fluid-structure interaction problem considered in the numerical simulations in the present paper.

For example, $A_\Psi A_\Phi G * \Phi$ can represent a dissipation effect, the origin of which is the energy release from S towards the environment E. In (Carcaterra et al., 2015), the case of radiation of waves generated by a mass-spring system (S) into a fluid-structure coupling (the environment E) is illustrated. Analogously, in (Carcaterra & Akay, 2011) the transmission of energy from a large master oscillator (the system S) to a set of small resonators (the environment E) is investigated, leading in both cases to integro-differential equations.

This mechanism helps in understanding the physical interpretation of $A_\Psi A_\Phi G * \Phi$ as memory effect. For example, a wave radiation from S into E can produce, after a delay time τ, a wave reflected back at some boundaries of E. The wave of intensity Φ radiated from S enters E and, after it is reflected back by some boundaries of E, it re-enters S. Therefore, if the flying time of this wave is τ, at the time t a perturbation $\Phi(t - \tau)$ enters the system S producing a memory effect.

This physical and mathematical background can be applied to model: (I) solid's memory effects, (II) thermodynamics behaviour, and (III) fluid-structures interaction.

(I) Viscoelasticity, ranging from bio-mechanics to civil infrastructures (Al Azzawi et al., 2019; Babaei et al., 2017; Carcaterra et al., 2015; Zhou et al., 2016), involves the macroscopic stress of the material in response to the entire time history of the strain, as for the Boltzmann's formulation of hereditary elasticity (Carillo, 2017), replacing the
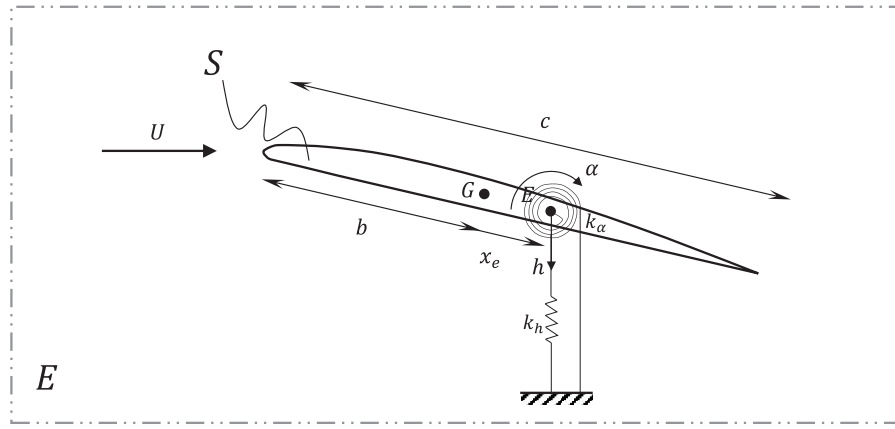
Figure 2. Aerofoil section geometry.

simple stress–strain proportionality, assumed in conventional elasticity, by a convolution stress–strain relationship. The creep response of materials is another example that makes use of the fractional hereditary model by Riemann-Liouville and Caputo's fractional derivative (Ahmad & Mohyud-Din, 2013; Caputo & Fabrizio, 2015), which again amounts to convolutional forms.

(II) The prototype Langevin's equation is another remarkable example, able to explain some features of irreversible processes and fluctuation-dissipation properties in the thermodynamics of the particle-bath interaction in the context of Brownian motion (Carcaterra & Akay, 2011). Finally, wave propagation in elastic meta-materials with long-range interactions, leads to superluminal group velocity, band gaps, or wave-stopping, as a direct consequence of the integro-differential formulation describing the travelling perturbations (Carcaterra et al., 2019; Rezaei et al., 2019).

(III) The convolution effects that are dealt with in this paper are aimed at the wake generation that the wing produces to generate lift and that are controlled by the control logic developed and proposed below. Integro-differential equations arise in many hydroelastic and aeroelastic problems including the structure-fluid coupling, as described by the Wagner theory of aerofoils due to the presence of a vortex wake (Carcaterra et al., 2005; Olsen & Wagner, 1982; Theodorsen, 1933). The vortex shedding at the wing tail produces a velocity perturbation about the wing by the vortices transported along the wake that, in turn, modify the wing lift as an effect of the past flow, generating a physical circuit with a delay, i.e. a memory effect.

In the case of the aerofoil, the wing is the system S, i.e a rigid body elastically restrained. The wing oscillates in a fluid flow that is the environment E. The general approach to the problem would be that of writing the equation of the fluid (e.g. the Navier-Stokes equations) in terms of the flow velocity, the variable Ψ, and the equation of the rigid body motion of the wing (see Figure 2), in terms of the plunge and pitch motion of the aerofoil, the variables Φ. Clearly, the coupling between S and E passes through interface continuity conditions that impose the fluid velocity at any point of the wing surface equal to that of the

wing, and the total interaction force (i.e. the local pressure and shear fluid viscous stress) produces the torque and the vertical force exciting the wing.

However, the equations of the wing, after very long mathematics, follow only in terms of the aerofoil variables, pitch, and plunge, making the fluid velocity field variable disappear, i.e. it is the hidden variable. The resulting equation of the wing, represented for example by the Wagner theory used in this paper, is integro-differential, the integral part taking into account the interaction with the fluid.

The proposed common origin of the convolution terms to describe the interaction of the studied system S with an external environment E, not directly modelled, and the general importance and diffusion of such integro-differential models in many disciplines, suggest the correspondent relevance of their analysis in the context of control.

3. Optimal controls of convolution-type integro-differential equations

Let us consider an integro-differential equation involving Volterra's kernel K:

$$\dot{x} = Ax + K * x + Bu \tag{3}$$

where $x(t)$ is the state vector, $A \in \mathbb{R}^{N \times N}$ the dynamic matrix, $u(t)$ the control variable, $B \in \mathbb{R}^{N \times M}$ the control matrix. The elements of K, $k_{ij}(t)$, are, in general, time-dependent, and (Einstein's notation is used):

$$(K * x)_i = \int_0^t k_{ij}(t - \tau) x_j(\tau) d\tau \quad i = 1, \ldots, N \tag{4}$$

introducing memory effects in the equation of motion.

Note that in several important physical applications (e.g. the case of the fluttering wing analyzed ahead), the kernel K can be expressed through exponential functions, i.e.:

$$k_{ij}(t) = \sum_{k=1}^{N} \alpha_{ijk} e^{-\beta_{ijk} t} \tag{5}$$

where α_{ijk} and β_{ijk} are characteristic coefficients of the model.
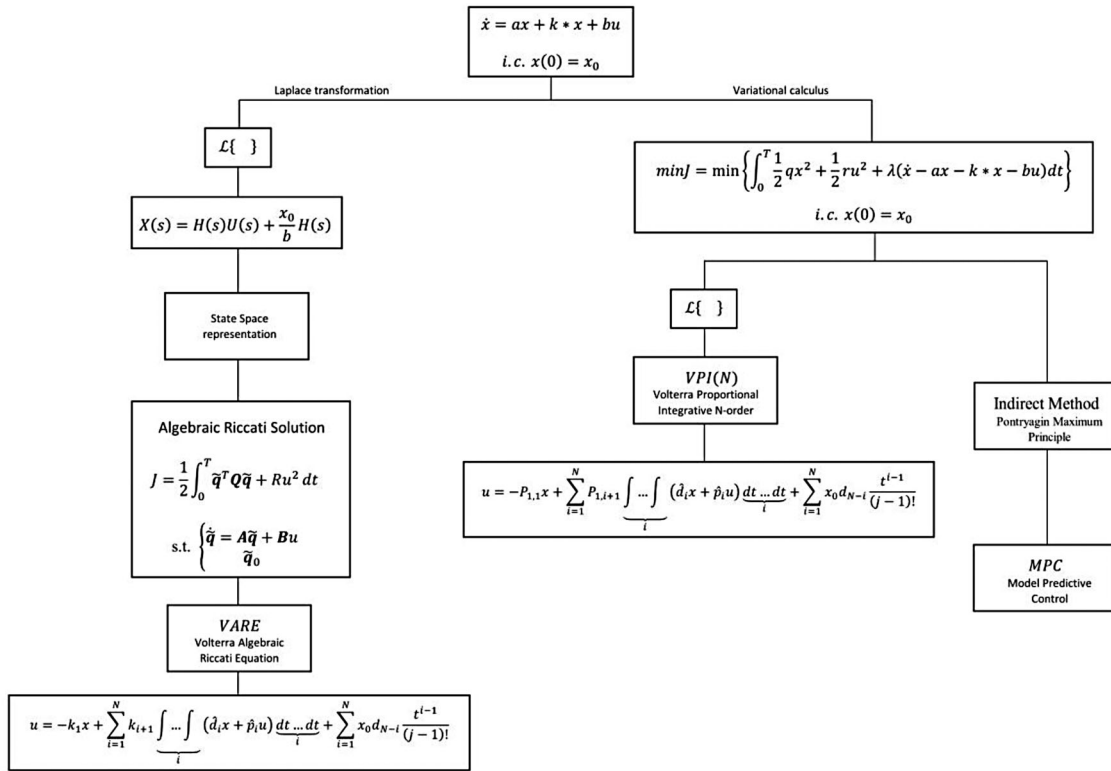
Figure 3. General scheme of the different proposed feedback control solutions for a scalar IDE.

This implies the memory effect decays as time is spent, making the more recent memory contributions larger with respect to the older ones, as intuitive.

For example, in fluidynamics, experimental studies by Jones (Jones, 1940) have shown that wake memory effects can be indeed represented by exponential functions. Similarly, in classical modelling of viscoelastic materials (Caputo & Fabrizio, 2015), Nutting demonstrates (Nutting, 1921) how hereditary Caputo's memory effects can be interpolated by exponentials. Exponentials are also the basis for hysteresis phenomena in modelling nonconventional constitutive relationships of materials (Mohammad Naser & Ikhouane, 2015).

Figure 3 shows the scheme of the two possible strategies of the solution to Equation (3) discussed ahead.

The first strategy, represented on the left side of the scheme, transforms directly Equation (3) into the Laplace domain – when its analytical form is available- and, after rearranging the equation in the Laplace domain, it transforms back to a first-order differential equation in the time domain, to which the LQR control applies.

The second strategy, represented on the right of the scheme, applies the variational approach to minimise the objective function, where the system's integro-differential equation is included in the objective function through the Lagrange multiplier. The equations produced by this minimisation are themselves integro-differential (Pontryagin, 2018). Then on the right part of the scheme, in turn, two possible solution strategies follow: (i) transform the problem into the Laplace domain if analytical expressions are available, as it happens for a kernel of exponential type considered here, or (ii) solve directly in the time domain, without particular hypotheses about the form of the kernel K.

This last solution is given in detail by the authors in and minimises the cost function:

$$J(\boldsymbol{x}, \boldsymbol{u}, \boldsymbol{\lambda}) = \int_0^T \frac{1}{2}\boldsymbol{x}^T \boldsymbol{Q}\boldsymbol{x} + \frac{1}{2}\boldsymbol{u}^T \boldsymbol{R}\boldsymbol{u}$$
$$+ \boldsymbol{\lambda}^T (\dot{\boldsymbol{x}} - \boldsymbol{A}\boldsymbol{x} - \boldsymbol{K} * \boldsymbol{x} - \boldsymbol{B}\boldsymbol{u})dt \qquad (6)$$

requiring $\delta J(\boldsymbol{x}, \boldsymbol{u}, \boldsymbol{\lambda}) = 0$. The non-standard term, the variation of $\boldsymbol{K} * \boldsymbol{x}$ with respect to $\boldsymbol{x}$, is one of the crucial aspects treated in (Yousefi et al., 2011). The minimisation problem finally leads to a set of integro-differential equations, the solution of which is in terms of $\boldsymbol{x}(t), \boldsymbol{u}(t), \boldsymbol{\lambda}(t)$, leading to an open loop control. In (Yousefi et al., 2011), the authors approach the solution by a model predictive control – MPC, a feedback method valid whatever the kernel $\boldsymbol{K}(t)$. Although very general, this method meets computational difficulties when the stiffness or dimension of the dynamic system increase (for more details see (Paifelman et al., 2021)).

To overcome this difficulty, in the present paper we simplify the problem assuming the exponential form of the kernel, as for Equation (3). Hence the chance to determine a feedback control without recurring to the MPC approach. This opens the way to a new opportunity of solution, named Volterra Proportional Integrative N-order VPI(N).

In fact, Equation (5) permits an analytical Laplace transform $\mathcal{L}\{\}$ of Equation (3):

$$\mathcal{L}\{k_{ij} * x_j\} = X_j(s) \sum_k \frac{\alpha_{ijk}}{s + \beta_{ijk}} = X_j(s) \frac{P_{ij}(N-1)(s)}{D_{ij}(N)(s)} \qquad (7)$$

where s is the Laplace variable, P_{ij} and D_{ij} are polynomials of order $N - 1$ and N, respectively.

3.1. Optimal control solution through the algebraic Riccati equation

Let us detail the procedure on the left side of Figure 3, treating for simplicity a scalar version of Equation (3):

$$\dot{x} = ax + \int_0^t K(t - \tau)x(\tau)d\tau + bu \qquad (8)$$

where $K(t) = \alpha_1 e^{-\beta_1 t}$, for $t \geq 0$, and $K(t) = 0$, for $t < 0$.

Laplace transform of Equation (8) produces:

$$sX(s) - x_0 = aX(s) + \frac{\alpha_1}{s + \beta_1}X(s) + bU(s) \qquad (9)$$

where $K(s) = \frac{\alpha_1}{s+\beta_1}$ and x_0 is the assigned initial condition. Rearranging the equation:

$$(sX(s) - x_0) + (sX(s) - x_0)\frac{\beta_1}{s}$$

$$= \left(aX(s) + aX(s)\frac{\beta_1}{s}\right) + \frac{\alpha_1 X(s)}{s} + \left(bU(s) + bU(s)\frac{\beta_1}{s}\right) \qquad (10)$$

Transforming back to the time domain:

$$\dot{x} = ax + (a\beta_1 + \alpha_1)\int_0^t x d\tau + bu + b\beta_1 \int_0^t u d\tau - \beta_1 x + x_0\beta_1 \qquad (11)$$

The integro-differential equation can now be traced back to the expanded state space by the change of coordinates $\tilde{q}_1 = x$, $\tilde{q}_2 = (a\beta_1 + \alpha_1)\int_0^t x d\tau + b\beta_1 \int_0^t u d\tau + x_0\beta_1$:

$$\begin{cases} \dot{\tilde{q}}_1 = a\tilde{q}_1 - \beta_1\tilde{q}_1 + \tilde{q}_2 + bu \\ \dot{\tilde{q}}_2 = (a\beta_1 + \alpha_1)\tilde{q}_1 + b\beta_1 u \end{cases} \qquad (12)$$

or using $\tilde{q} = [\tilde{q}_1 \, \tilde{q}_2]^T$:

$$\dot{\tilde{q}} = A\tilde{q} + Bu$$

$$A = \begin{bmatrix} a - \beta_1 & 1 \\ a\beta_1 + \alpha_1 & 0 \end{bmatrix}, B = \begin{bmatrix} b \\ b\beta_1 \end{bmatrix} \qquad (13)$$

The optimal control solution can be now easily found through the application of the Linear Quadratic Regulator which solves the classic Algebraic Riccati Equations thus obtaining the control solution as:

$$u = -K\tilde{q}$$

$$= -k_1 x - k_2\left((a\beta_1 + \alpha_1)\int_0^t x d\tau + b\beta_1 \int_0^t u d\tau + x_0\beta_1\right) \qquad (14)$$

with $K = [k_1 k_2]$ the optimal gain matrix $\mathbb{R}^{1 \times 2}$ that minimises the quadratic cost function:

$$J = \frac{1}{2}\int_0^T \tilde{q}^T Q\tilde{q} + Ru^2 dt \qquad (15)$$

with $Q \in \mathbb{R}^{2 \times 2}$ and R tuning parameters.

Equation (14) represents the searched feedback control and it stands in the form of an integral equation of Volterra-type in terms of the control output u, below named Volterra Algebraic Riccati Equation -VARE, and is one of the central results of the present paper. The numerical solution of this equation is at hand and does not present any particular difficulty.

A generalisation of this approach to the matrix case, i.e. $N > 1$, is presented in Appendix A.

3.2. Optimal control solution by variational calculus

Let us follow the right branch of Figure 3, first applying the calculus of the variations and then transforming it into the Laplace domain. The minimisation of the objective function (6), in its scalar form, implies:

$$\min\left\{J = \int_0^T \frac{1}{2}qx^2 + \frac{1}{2}ru^2 + \lambda(\dot{x} - ax - k * x - bu)dt\right\}$$

$$i.c.x(0) = x_0 \qquad (16)$$

and for $\delta J = 0$, one obtains the integro-differential problem:

$$\begin{cases} \dot{x} = ax + \lambda\frac{b^2}{r} + \int_0^\infty k(t - \tau)x(\tau)d\tau \\ \dot{\lambda} = qx - a\lambda - \int_0^\infty k(\tau - t)\lambda(\tau)d\tau \\ \lim_{T \to \infty} \lambda(T) = 0, \quad x(0) = x_0, u = \frac{b}{r}\lambda \end{cases} \qquad (17)$$

The existence of the transversality conditions at two opposite boundaries $\lambda(T) = 0$, $x(0) = x_0$, precludes the chance of any direct feedback control. The proposed method, here called Volterra Proportional Integrative N-order, VPI(N), supports a feedback solution through a particular form of the kernel and the Lagrange multiplier.

Laplace transform of Equations (17) -considering for simplicity $N = 1$ in equation (5), produces:

$$sX(s) - x_0 = aX(s) + \frac{b^2}{r}\Lambda(s) + \frac{\alpha_1}{s + \beta_1}X(s)$$

$$s\Lambda(s) - \lambda_0 = qX(s) - a\Lambda(s) - \frac{\alpha_1}{s - \beta_1}\Lambda(s) \qquad (18)$$

and rearranging:

$$(sX(s) - x_0) = (a - \beta_1)X(s) + \frac{b^2}{r}\Lambda(s) + \frac{a\beta_1 + \alpha_1}{s}X(s)$$

$$+ \frac{b^2\beta_1}{rs}\Lambda(s) + x_0\frac{\beta_1}{s}$$

$$(s\Lambda(s) - \lambda_0) = qX(s) - (a - \beta_1)\Lambda(s) - q\frac{\beta_1}{s}X(s)$$

$$+ \frac{a\beta_1 - \alpha_1}{s}\Lambda(s) - \lambda_0\frac{\beta_1}{s} \qquad (19)$$

Laplace anti-transform $\mathcal{L}^{-1}\{\}$ and the introduction of the new variables $\boldsymbol{\xi} = [\xi_1, \xi_2]^T$, $\boldsymbol{\eta} = [\eta_1, \eta_2]^T$, defined as

$$\boldsymbol{\xi} = \begin{bmatrix} \xi_1 \\ \xi_2 \end{bmatrix}$$
$$= \begin{bmatrix} x \\ a\beta_1 \int_0^t x(\tau)d\tau + \frac{b^2}{r}\beta_1 \int_0^t \lambda(\tau)d\tau + \alpha_1 \int_0^t x(\tau)d\tau + x_0\beta_1 \end{bmatrix}$$

$$\boldsymbol{\eta} = \begin{bmatrix} \eta_1 \\ \eta_2 \end{bmatrix}$$
$$= \begin{bmatrix} \lambda \\ -q\beta_1 \int_0^t x(\tau)d\tau + a\beta_1 \int_0^t \lambda(\tau)d\tau - \alpha_1 \int_0^t \lambda(\tau)d\tau - \lambda_0\beta_1 \end{bmatrix}$$

$$(20)$$

produces:

$$\dot{\boldsymbol{\xi}} = \begin{bmatrix} a - \beta_1 & 1 \\ a\beta_1 + \alpha_1 & 0 \end{bmatrix}\boldsymbol{\xi} + \begin{bmatrix} \frac{b^2}{r} & 0 \\ \frac{b^2}{r}\beta_1 & 0 \end{bmatrix}\boldsymbol{\eta}$$

$$\dot{\boldsymbol{\eta}} = \begin{bmatrix} q & 0 \\ -q\beta_1 & 0 \end{bmatrix}\boldsymbol{\xi} + \begin{bmatrix} (\beta_1 - a) & 1 \\ a\beta_1 - \alpha_1 & 0 \end{bmatrix}\boldsymbol{\eta} \qquad (21)$$

or assembling in a compact form:

$$\begin{cases} \dot{\boldsymbol{\xi}} = \boldsymbol{H}_{\xi\xi}\boldsymbol{\xi} + \boldsymbol{H}_{\xi\eta}\boldsymbol{\eta} \\ \dot{\boldsymbol{\eta}} = \boldsymbol{H}_{\eta\xi}\boldsymbol{\xi} + \boldsymbol{H}_{\eta\eta}\boldsymbol{\eta} \end{cases} \qquad (22)$$

that reduces the integro-differential Equation (17) to a first-order differential equation.

The generalised Hamiltonian matrices $\boldsymbol{H}_{ij}$ depend on the coefficients α_i and β_i that characterise the kernel $k(t)$. The control $u(t)$ is simply proportional to $\lambda(t)$, as reported by the third of eq (17), i.e.:

$$u(t) = \frac{b}{r}\lambda(t) \qquad (23)$$

Therefore, from Equation (22) it is sufficient to determine the solution $\lambda(t)$ to produce the control u. The great advantage of Equation (22) with respect to Equation (17) is that from Equation (22) we determine a feedback solution $u = \frac{b}{r}\lambda(x)$. This goal is achieved by looking for solutions of the form:

$$\boldsymbol{\eta} = \boldsymbol{P}\boldsymbol{\xi} \qquad (24)$$

with matrix $\boldsymbol{P} \in \mathbb{R}^{2\times 2}$ that produces

$$\begin{cases} \dot{\boldsymbol{\xi}} = \boldsymbol{H}_{\xi\xi}\boldsymbol{\xi} + \boldsymbol{H}_{\xi\eta}\boldsymbol{P}\boldsymbol{\xi} \\ \dot{\boldsymbol{P}}\boldsymbol{\xi} + \boldsymbol{P}\dot{\boldsymbol{\xi}} = \boldsymbol{H}_{\eta\xi}\boldsymbol{\xi} + \boldsymbol{H}_{\eta\eta}\boldsymbol{P}\boldsymbol{\xi} \end{cases} \qquad (25)$$

and its compatibility condition:

$$\dot{\boldsymbol{P}} + \boldsymbol{P}\boldsymbol{H}_{\xi\xi} + \boldsymbol{P}\boldsymbol{H}_{\xi\eta}\boldsymbol{P} - \boldsymbol{H}_{\eta\xi} - \boldsymbol{H}_{\eta\eta}\boldsymbol{P} = 0 \qquad (26)$$

This is the generalised Riccati's nonstationary equation associated with the original integro-differential problem (17).

It is known that solutions of the general Riccati equation are not available for a feedback formulation, and only special cases can be treated. For this reason, we consider its stationary form:

$$\boldsymbol{P}\boldsymbol{H}_{\xi\xi} + \boldsymbol{P}\boldsymbol{H}_{\xi\eta}\boldsymbol{P} - \boldsymbol{H}_{\eta\xi} - \boldsymbol{H}_{\eta\eta}\boldsymbol{P} = 0 \qquad (27)$$

Note the matrix $\boldsymbol{H}_{(4x4)} = [\boldsymbol{H}_{\xi\xi}\boldsymbol{H}_{\xi\eta}; \boldsymbol{H}_{\eta\xi}\boldsymbol{H}_{\eta\eta}]$ is not Hamiltonian, because $(\boldsymbol{JH})^T \neq \boldsymbol{JH}$, where $\boldsymbol{J}$ is representing a generical skew-symmetric matrix. For this reason, difficulties arise in the solution of Equation (26) by using classical approaches. However, a solution of (26) can be determined by looking at the eigenvalues problem of the matrix $\boldsymbol{H}$.

Introducing the vector $\boldsymbol{v} = [\boldsymbol{\xi}, \boldsymbol{\eta}]^T$, Equation (22) can be written as:

$$\dot{\boldsymbol{v}} = \boldsymbol{H}\,\boldsymbol{v} \qquad (28)$$

and its general solution can be expressed in function of its 4 eigenvectors $\boldsymbol{\psi}_k\boldsymbol{\theta}_k$ and eigenvalues $\boldsymbol{p} = [p_1, \ldots, p_4]$ by using the modal expansion:

$$\boldsymbol{v} = \begin{bmatrix} \xi \\ \eta \end{bmatrix} = \sum_{k=1}^{4} c_k \begin{bmatrix} \boldsymbol{\psi}_k \\ \boldsymbol{\theta}_k \end{bmatrix} e^{p_k t} \qquad (29)$$

where the c_k are the coefficients to be determined by imposing the initial and final boundary conditions.

Splitting the summation, separating the eigenvalues p_k with positive real part from those negative, Equation (29) can be written as:

$$\boldsymbol{v} = \begin{bmatrix} \xi \\ \eta \end{bmatrix} = \sum_{k=1}^{J} c_k^{\{1\}} \begin{bmatrix} \boldsymbol{\psi}_k^{\{1\}} \\ \boldsymbol{\theta}_k^{\{1\}} \end{bmatrix} e^{p_k^{\{1\}} t} + \sum_{k=1}^{R} c_k^{\{2\}} \begin{bmatrix} \boldsymbol{\psi}_k^{\{2\}} \\ \boldsymbol{\theta}_k^{\{2\}} \end{bmatrix} e^{p_k^{\{2\}} t}$$

$$(30)$$

where $J + R = 4$, the superscript $\{1\}$ identifies the set $\boldsymbol{\psi}_k, \boldsymbol{\theta}_k, c_k$ associated to $\mathcal{R}e\{p_k\} \geq 0$, the superscript $\{2\}$ to $\mathcal{R}e\{p_k\} < 0$, respectively.

In general, in the modal expansion (30), one needs to determine $c_k^{\{1\}}, c_k^{\{2\}}$, respecting the boundary conditions.

Since one requires the final condition $\lim_{T\to\infty} \lambda(T) = 0$ holds, then $c_k^{\{1\}} = 0$, to cancel out the diverging exponential terms, at the same time preventing the system instability. Therefore:

$$\begin{bmatrix} \xi \\ \eta \end{bmatrix} = \sum_{k=1}^{R} c_k^{\{2\}} \begin{bmatrix} \boldsymbol{\psi}_k^{\{2\}} \\ \boldsymbol{\theta}_k^{\{2\}} \end{bmatrix} e^{p_k^{\{2\}} t} \qquad (31)$$

Introducing the vector

$$\boldsymbol{c}^{\{2\}} = \left[c_1^{\{2\}}, \ldots, c_R^{\{2\}} \right]^T \qquad (32)$$

one obtains:

$$\begin{cases} \boldsymbol{\xi} = \boldsymbol{\Psi}^{\{2\}}\boldsymbol{E}\boldsymbol{c}^{\{2\}} \\ \boldsymbol{\eta} = \boldsymbol{\Theta}^{\{2\}}\boldsymbol{E}\boldsymbol{c}^{\{2\}} \end{cases} \qquad (33)$$

where:

$$\boldsymbol{\Psi}^{\{2\}} = \begin{bmatrix} \boldsymbol{\psi}_1^{\{2\}} & \cdots & \boldsymbol{\psi}_R^{\{2\}} \end{bmatrix}$$

$$\boldsymbol{\Theta}^{\{2\}} = \begin{bmatrix} \boldsymbol{\theta}_1^{\{2\}} & \cdots & \boldsymbol{\theta}_R^{\{2\}} \end{bmatrix} \qquad (34)$$

are 2xR matrices, and E is the RxR diagonal matrix:

$$E = \begin{bmatrix} e^{p_1 t} & 0 & 0 \\ 0 & \ldots & 0 \\ 0 & 0 & e^{p_R t} \end{bmatrix} \tag{35}$$

Let us examine the initial conditions to determine $c_k^{\{2\}}$. At $t = 0$ we have:

$$\boldsymbol{\xi}_0 = \begin{bmatrix} x_0 \\ x_0 \beta_1 \end{bmatrix}, \boldsymbol{\eta}_0 = \begin{bmatrix} \lambda_0 \\ -\lambda_0 \beta_1 \end{bmatrix} \tag{36}$$

that implies:

$$\begin{cases} \boldsymbol{\xi}_0 = \boldsymbol{\Psi}^{\{2\}} \boldsymbol{c}^{\{2\}} \\ \boldsymbol{\eta}_0 = \boldsymbol{\Theta}^{\{2\}} \boldsymbol{c}^{\{2\}} \end{cases} \tag{37}$$

Now if $R = 2 = J$, then the matrix $\boldsymbol{\Psi}^{\{2\}}$ is a squared one, and assuming it is invertible, we can express the coefficient of the modal expansion as:

$$\boldsymbol{c}^{\{2\}} = \boldsymbol{\Psi}^{\{2\}-1} \boldsymbol{\xi}_0 \tag{38}$$

Therefore:

$$\boldsymbol{\eta} = \boldsymbol{\Theta}^{\{2\}} \boldsymbol{E} \boldsymbol{c}^{\{2\}} = \boldsymbol{\Theta}^{\{2\}} \boldsymbol{E} \boldsymbol{\Psi}^{\{2\}-1} \boldsymbol{\xi}_0$$

$$\boldsymbol{\xi} = \boldsymbol{\Psi}^{\{2\}} \boldsymbol{E} \boldsymbol{c}^{\{2\}} = \boldsymbol{\Psi}^{\{2\}} \boldsymbol{E} \boldsymbol{\Psi}^{\{2\}-1} \boldsymbol{\xi}_0 \rightarrow \boldsymbol{E} \boldsymbol{\Psi}^{\{2\}-1} \boldsymbol{\xi}_0 = \boldsymbol{\Psi}^{\{2\}-1} \boldsymbol{\xi} \tag{39}$$

that implies:

$$\boldsymbol{\eta} = \boldsymbol{\Theta}^{\{2\}} \boldsymbol{\Psi}^{\{2\}-1} \boldsymbol{\xi} = \boldsymbol{P} \boldsymbol{\xi} \tag{40}$$

that is the desired feedback control form of Equation (24).

If $R \neq J$, the matrix $\boldsymbol{\Psi}^{\{2\}}$ is rectangular and not invertible, and Equation (40) is not valid anymore. However, an approximated approach could use the pseudo-inverse matrix $\boldsymbol{\Psi}^{\{2\}+}$:

$$\boldsymbol{\eta} = \boldsymbol{\Theta}^{\{2\}} \boldsymbol{\Psi}^{\{2\}+} \boldsymbol{\xi} = \boldsymbol{P} \boldsymbol{\xi} \tag{41}$$

which only guarantees the determined solution is optimal in the least square sense (if $R < J$) or minimum norm sense (if $R > J$).

For both Equations (40) and (41), the explicit control law for u is determined using only the first row of (24):

$$u = \frac{b}{r} \left\{ P_{1,1} x + P_{1,2} \left[(a\beta_1 + \alpha_1) \int x dt + b\beta_1 \int u dt + x_0 \beta_1 \right] \right\} \tag{42}$$

where $[P_{1,1}, P_{1,2}]$ are indicating the first row elements of the $\boldsymbol{P}$ matrix.

Equation (42) is again an integral equation of Volterra, in terms of the control variable u, the same found for the left branch of paragraph 3.1, see Equation (14), except for the values of the coefficients related to the K matrix, which come from the P matrix solution for the VPI(N) controller. Equation (42), together with Equation (14), is the central contribution of this paper.

The general method based on an exponential series of the kernel for $N > 1$ is illustrated in Appendix B.

Table 1. Parameters settings used to compare VPI(N) and VARE algorithms.

Parameters	Values
a	-0.1
b	1
α_1	-8.19
β_1	5.28
x_0	1
Q_1	10
Q_2	$\in [0; 1]$
r	0.05
$[p_1, p_2, p_3, p_4]$	$[-13.9; 14.4; -5.5; 4.9]$
$\Psi^{\{2\}}$	$\begin{bmatrix} 0.13 & -0.02 \\ 0.81 & -0.95 \end{bmatrix}$
$\Theta^{\{2\}}$	$\begin{bmatrix} -0.09 & 0.04 \\ 0.55 & -0.28 \end{bmatrix}$

4. Numerical results

In this section, the control approaches illustrated in Section 3.1 and 3.2 are compared using numerical simulations. A first comparison is made for a scalar prototype of IDE without any particular physical meaning. The second comparison represents instead an elastic wing with the vortex wake. The wing, elastically restrained, vibrates under the action of the fluid. This is a typical engineering problem of dynamic instability that will be controlled here by VARE and VPI(N) methods.

4.1. Case study of a scalar IDE

Let's start with the simplest model

$$\dot{x} = ax + \int_0^t K(t - \tau) x(\tau) d\tau + bu \tag{43}$$

with $K(t) = \alpha_1 e^{-\beta_1 t}$.

A direct comparison between the two proposed controllers in terms of the cost function J is not obvious because the VARE minimises $J = \frac{1}{2} \int_0^T \tilde{\boldsymbol{q}}^T \boldsymbol{Q} \tilde{\boldsymbol{q}} + ru^2 dt$, while VPI(N) minimise $sJ = \int_0^T \frac{1}{2} Q_1 x^2 + \frac{1}{2} ru^2$.

To remedy this, we have chosen to use the J's VPI(N) and therefore the VARE matrix $\boldsymbol{Q}$ contains the same gain Q_1 of VPI(N) and an additional parameter of tuning Q_2:

$$\boldsymbol{Q} = \begin{bmatrix} Q_1 & 0 \\ 0 & Q_2 \end{bmatrix} \tag{44}$$

The simulations are performed with the parameters listed in Table 1, where Q_1 and r are set out to reach the behaviour of the VPI(N) method as close as possible to the Pontryagin solution, and Q_2 belongs to the interval $[0; 1]$.

Figures 4 – 6 show the comparison in terms of state, control, and cost function for the two controllers.

For Q_2 close to 1, the VPI(N) provides results much closer to the optimal Pontryagin solution, with respect to the VARE method. The VARE becomes comparable with the Pontryagin solution for Q_2 small enough, finding a perfect matching for $Q_2 = 0$.
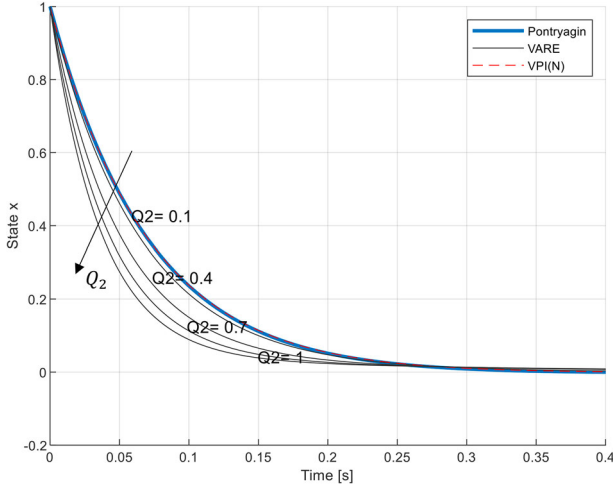
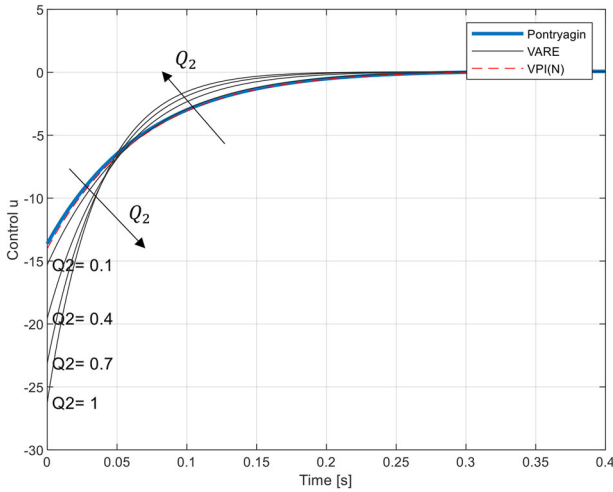**Figure 4.** State x for VPI(N) vs VARE method with variable Q_2.

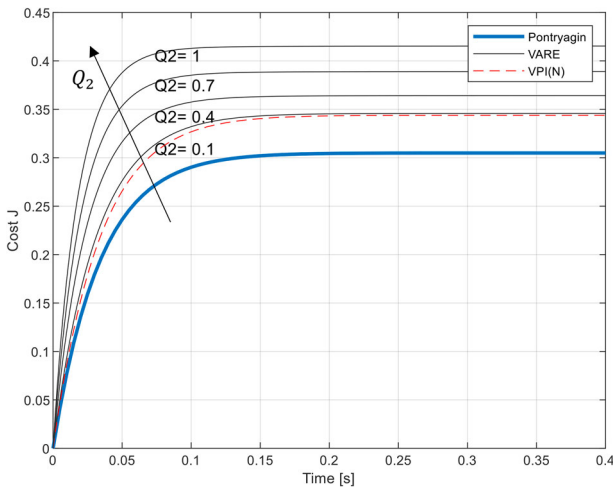**Figure 5.** Control u for VPI(N) vs VARE method with variable Q_2.

Figure 6. Cost function J for VPI(N) vs VARE with variable Q_2.

4.2. Case study of an unsteady airfoil dynamic

In this section, the proposed control algorithms are tested for a typical engineering problem: the flutter and static instabilities of an aerofoil by using the classical aerodynamic model by

Wagner and Jones (Jones, 1940; Olsen & Wagner, 1982). A wing immersed within a constant speed current flow U is subject to a downwash burst. The latter creates a non-stationary aerodynamic force and if the inflow speed exceeds a critical value, i.e. it makes the wing unstable, resulting in large oscillations of the wing response that diverges.

Let us consider a two-degree of freedom aerofoil, and denote the plunge by $h(t)$ and the pitch by $\alpha(t)$, respectively. Figure 2 shows the aerofoil section where the chord is $c = 2b$, and G, E and x_e are the gravity centre, the elastic centre, and the distance GE, respectively.

The typical two-dimensional wing equations of motion are:

$$\begin{bmatrix} m_w & S_w \\ S_w & I_w \end{bmatrix} \ddot{q} + \begin{bmatrix} k_h & 0 \\ 0 & k_\alpha \end{bmatrix} q = \begin{bmatrix} -L_C(t) - L_{NC}(t) \\ M_C(t) + M_{NC}(t) \end{bmatrix} \quad (45)$$

where m_w, I_w, S_w, k_h and k_α are the mass, inertia, static moment, plunge, and pitch stiffness, respectively. The state vector is $q = [h, \alpha]^T$ and the aerodynamic external forces, formulated by Wagner and Jones (Jones, 1940; Olsen & Wagner, 1982) are the lift $L(t)$ and torque $M(t)$. The forces are composed by the non-circulatory hydrodynamic contribute (NC) and the circulatory one (C). The non-circulatory terms, named apparent mass forces, are expressed as:

$$L_{NC} = \pi \rho s b^2 \left[\ddot{h} + U\dot{\alpha} - x_e \ddot{\alpha} \right] \quad (46)$$

$$M_{NC} = \pi \rho s b^2 \left[x_e \ddot{h} - Ub \left(\frac{1}{2} - \frac{x_e}{b} \right) \dot{\alpha} - b^2 \left(\frac{1}{8} + \frac{x_e^2}{b^2} \right) \ddot{\alpha} \right] \quad (47)$$

where ρ and s are the flow density and wingspan. The presence of a circulatory contribution, physically related to the vortex shedding, implies the presence of a convolution term, which represents the memory effects (see (Jones, 1940) for more details). The circulatory lift and torque are:

$$L_C = 2\pi s \rho Ub \left[w(0)\phi(t) + \int_0^t \dot{w}(\tau)\phi(t - \tau)d\tau \right] \quad (48)$$

$$M_C = b \left[\frac{1}{2} + \frac{x_e}{b} \right] L_C \quad (49)$$

where $w(t) = U\alpha(t) + \dot{h}(t) + \dot{\alpha}(t) \left(\frac{1}{2} - \frac{x_e}{b} \right) b$ is the downwash composed of (i) uniform downwash corresponding to a pitching angle α, $w = U\sin(\alpha) \approx U\alpha$ for small angles; (ii) a uniform downwash due to the vertical translation $\dot{h}$; (iii) and a non-uniform downwash $\dot{\alpha}$ evaluated at $\frac{3}{4}$ -chord. Finally

$$\phi(t) = 1 - \psi_1 e^{-\frac{\varepsilon_1 U}{b}t} - \psi_2 e^{-\frac{\varepsilon_2 U}{b}t} \quad (50)$$

is the Wagner function approximated as in (Jones, 1940).

By substituting the expressions from (46) to (49) into Equation (45), we obtain the classical formulation of the integral differential equation:

$$M\ddot{q} + Kq + C\dot{q} = F \ast \dot{\phi} \quad (51)$$

where the matrices which represent mass M, stiffness K, and damping C of the system and the circulatory forces $F \ast \dot{\phi}$ have

the detailed mathematical forms:

$$M = \begin{bmatrix} m_w + \pi s\rho b^2 & S_w - \pi s\rho b^2 x_e \\ S_w - \pi s\rho b^2 x_e & I_w + \pi s\rho b^4 \left(\frac{1}{8} + \frac{x_e^2}{b^2} \right) \end{bmatrix}$$

$$K = \begin{bmatrix} k_h & 2\pi s\rho U^2 b\phi(0) \\ 0 & k_\alpha - 2\pi s\rho U^2 b^2 \left[\frac{1}{2} + \frac{x_e}{b} \right] \phi(0) \end{bmatrix}$$

$$C = \begin{bmatrix} 2\pi s\rho U b\phi(0) \\ -2\pi s\rho U b^2 \left[\frac{1}{2} + \frac{x_e}{b} \right] \phi(0) \end{bmatrix}$$

$$\times \begin{bmatrix} 2\pi s\rho U b^2 \left(\frac{1}{2} - \frac{x_e}{b} \right) \phi(0) + \pi s\rho U b^2 \\ \pi s\rho U b^3 \left(\frac{1}{2} - \frac{x_e}{b} \right) \left(1 - \left[1 + \frac{2x_e}{b} \right] \phi(0) \right) \end{bmatrix}$$

$$F*\dot{\phi} = \begin{bmatrix} -2\pi s\rho U b \int_0^t \left(U\alpha(\tau) + \dot{h}(\tau) \right. \\ \left. + \dot{\alpha}(\tau) \left(\frac{1}{2} - \frac{x_e}{b} \right) b \right) \dot{\phi}(t-\tau) d\tau \\ 2\pi s\rho U b^2 \left[\frac{1}{2} + \frac{x_e}{b} \right] \int_0^t \left(U\alpha(\tau) + \dot{h}(\tau) \right. \\ \left. + \dot{\alpha}(\tau) \left(\frac{1}{2} - \frac{x_e}{b} \right) b \right) \dot{\phi}(t-\tau) d\tau \end{bmatrix} \quad (52)$$

Let us define the state vector as $x = [q, \dot{q}]^T$ and insert a control u proportional to the torque acting on the wing pitch. The equation of motion is:

$$\dot{x} = Ax + Dx * \dot{\phi} + Bu \quad (53)$$

where the matrices definition are reported below (I is the identity matrix):

$$A = \begin{bmatrix} 0 & I \\ -M^{-1}K & -M^{-1}C \end{bmatrix},$$

$$D = \begin{bmatrix} 0 & 0 \\ M^{-1}D_1 & M^{-1}D_2 \end{bmatrix}, B = \begin{bmatrix} 0 \\ 0 \\ 0 \\ 1 \end{bmatrix}$$

$$D_1 = \begin{bmatrix} 0 & -2\pi s\rho U^2 b \\ 0 & 2\pi s\rho U^2 b^2 \left[\frac{1}{2} + \frac{x_e}{b} \right] \end{bmatrix}$$

$$D_2 = \begin{bmatrix} -2\pi s\rho U b \\ 2\pi s\rho U b^2 \left[\frac{1}{2} + \frac{x_e}{b} \right] \end{bmatrix}$$

$$\times \begin{bmatrix} -2\pi s\rho U b^2 \left(\frac{1}{2} - \frac{x_e}{b} \right) \\ 2\pi s\rho U b^3 \left[\frac{1}{2} + \frac{x_e}{b} \right] \left(\frac{1}{2} - \frac{x_e}{b} \right) \end{bmatrix} \quad (54)$$

In the next sections, the model of the wing represented by Equation (53) is controlled both through the VARE and the VPI(N) control techniques, respectively.

The next two subsections specify the mathematical formulation of the control algorithms for the wing case, as it comes out from the previous theory.

4.2.1. VARE control algorithm formulation
Following the procedure illustrated in the previous part of the paper, the expanded state-space dynamic permits to write the first order equation of motion of the wing as

$$\dot{\tilde{q}} = \tilde{A}\tilde{q} + \tilde{B}u \quad (55)$$

where:

$$\tilde{A} = \begin{bmatrix} (A - Id_1) & I & 0 \\ Ad_1 + Dp_1 - Id_0 & 0 & I \\ Ad_0 + Dp_0 & 0 & 0 \end{bmatrix}, \tilde{B} = \begin{bmatrix} B \\ Bd_1 \\ Bd_0 \end{bmatrix} \quad (56)$$

and the state variable $\tilde{q} = [\tilde{q}_1, \tilde{q}_2, \tilde{q}_3]^T$ is so organised:

$$\tilde{q}_1 = x$$

$$\tilde{q}_2 = \int_0^t d_1 Ax\, d\tau + \int_0^t p_1 Dx\, d\tau + \int_0^t Bd_1 u\, d\tau + x_0 d_1$$

$$- \int_0^t d_0 x\, d\tau + \int_0^t \int_0^\tau d_0 Ax\, d\tau\, d\tau' + \int_0^t \int_0^\tau p_0 Dx\, d\tau\, d\tau'$$

$$+ \int_0^t \int_0^\tau Bd_0 u\, d\tau\, d\tau' + x_0 d_0 t$$

$$\tilde{q}_3 = \int_0^t d_0 Ax\, d\tau + \int_0^t p_0 Dx\, d\tau + \int_0^t d_0 Bu\, d\tau + x_0 d_0 \quad (57)$$

with $d_0 = \varepsilon_1 \varepsilon_2 \left(\frac{2U}{c} \right)^2$, $d_1 = (\varepsilon_1 + \varepsilon_2) \left(\frac{2U}{c} \right)$, $p_0 = \varepsilon_1 \varepsilon_2 (\psi_1 + \psi_2) \left(\frac{2U}{c} \right)^2$ and $p_1 = (\varepsilon_1 \psi_1 + \varepsilon_2 \psi_2) \left(\frac{2U}{c} \right)$.

Let us minimise the classic quadratic cost function:

$$J = \frac{1}{2} \int_0^T \tilde{q}^T Q\tilde{q} + Ru^2\, dt \quad (58)$$

and apply the stationary Riccati solution obtaining:

$$u = -K\tilde{q} \quad (59)$$

where K is the optimal gain matrix. Equation (59) is an integral Volterra's equation in terms of u to be solved numerically.

4.2.2. VPI(N) control algorithm formulation
The VPI(N) control algorithm follows the variational formulation of Equation (53)

$$\dot{x} = Ax + Dx*\dot{\phi} + BR^{-T}B^T\lambda$$
$$\dot{\lambda} = Q^T x - A^T\lambda - D^T\lambda * \dot{\phi} \quad (60)$$

its compact is

$$\begin{cases} \dot{\xi} = H_{\xi\xi}\xi + H_{\xi\eta}\eta \\ \dot{\eta} = H_{\eta\xi}\xi + H_{\eta\eta}\eta \end{cases} \quad (61)$$

where the $H_{ij} \in \mathbb{R}^{12 \, 12}$ matrixes are expressed as follows:

$$H_{\xi\xi} = \begin{bmatrix} (A - Id_1) & I & 0 \\ Ad_1 + Dp_1 - Id_0 & 0 & I \\ Ad_0 + Dp_0 & 0 & 0 \end{bmatrix} \quad H_{\xi\eta} = \begin{bmatrix} BR^{-T}B^T & 0 \\ BR^{-T}B^T d_1 & 0 \\ BR^{-T}B^T d_0 & 0 \end{bmatrix}$$

$$H_{\eta\eta} = \begin{bmatrix} (-A^T - Id_1) & I & 0 \\ -A^T d_1 - D^T d_1 - Id_0 & 0 & I \\ -A^T d_0 - D^T d_0 & 0 & 0 \end{bmatrix} \quad H_{\eta\xi} = \begin{bmatrix} Q^T & 0 \\ Q^T d_1 & 0 \\ Q^T d_0 & 0 \end{bmatrix} \tag{62}$$

As for the Equation (42), the final control law takes the form:

$$\begin{aligned} u = R^{-T}B^T\lambda = P_{11}x &+ P_{12}\left(\int Ad_1 x + \int p_1 Dx + \int Bd_1 u\right. \\ &+ x_0 d_1 - \int d_0 x + \int\int Ad_0 x + \int\int p_0 Dx + \int\int Bd_0 u \\ &+ \left. x_0 d_0 t\right) + P_{13}\left(\int Ad_0 x + \int p_0 Dx + \int Bd_0 u + x_0 d_0\right) \end{aligned} \tag{63}$$

an integral Volterra equation in terms of u, where P_{11}, P_{12}, P_{13} are the coefficients of Riccati's matrix, which is the solution of Equation (27) and x_0 is the assigned initial condition.

4.2.3. Numerical results and discussion

The two VPI(N) and VARE controls are compared below by analyzing different flight configurations and tuning parameters.

In particular, Wagner's wing exhibits a speed threshold, called flutter velocity, that when exceeded produces an unstable wing motion.

Looking at Figure 7, once the wing parameters have been set (see Table 2), three different regions can be highlighted, associated with three separated behaviours, depending on the ratio $\frac{x_e}{c}$ and the inflow speed U. More precisely, looking at Figure 7: (i) below the curve U_{flutter}, oscillations are always stable; (ii) at the top margin on the right, the divergent instability emerges, i.e. the average trend of the state (both pitch and plunge) shows a divergent trend; (iii) at the top margin of the left, a typical flutter vibration is shown, in which is the amplitude of oscillations (both pitch and plunge) diverges, while the average trend of the response remains neutral.

We investigate four different flight regimes, identified by the star marker symbols in the map of Figure 7. Two simulations relate to stable flight conditions, while the other two to divergent and fluttering instability, respectively. In Table 3, the reference data for the simulations are shown.
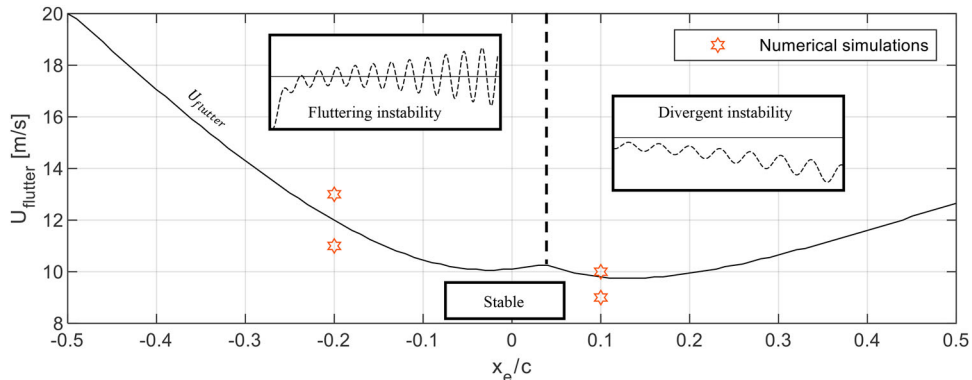
Table 2. Numerical simulation parameters.

Parameters		Values	
c	Chord	0.1	[m]
a	Thickness	0.005	[m]
s	Span	1	[m]
ρ	Density	2300	[kg/m^3]
f_h	Plunge frequency	1	[Hz]
f_α	Pitch frequency	5	[Hz]
m_w	Mass	1.15	[Kg]
I_w	Inertia	0.0011	[kg/m^2]
S_w	Static Moment	-0.0115	[kg m]
k_h	Plunge stiffness	45.4	[N/m]
k_α	Pitch stiffness	1.06	[Nm/rad]
$[\varepsilon_1; \psi_1; \varepsilon_2; \psi_2]$	Kernel parameters	[0.041; 0.165; 0.32; 0.335]	–

Table 3. Numerical simulations scenarios.

x_e/c	U_{flutter}	U_{inflow}
-0.2	12m/s	11m/s *(stable dynamic)*
		13m/s *(unstable dynamic)*
0.1	9.5m/s	9m/s *(stable dynamic)*
		10m/s *(unstable dynamic)*

In Table 4 are reported the settings for the two controllers, divided in two categories, for $\frac{x_e}{c} = -0.2$ and $\frac{x_e}{c} = 0.1$, respectively, and tested in both conditions of stability and dynamic instability. For all cases, the VPI(N) control is compared with the VARE. As previously observed, the latter exhibits more tuning parameters generated by the state expansion, and two sets of tuning for the VARE are tested, called set_1 and set_2, showing quite different trends.

The cost function, for both methods, is the one referred to the VPI(N), so defined:

$$J = \frac{1}{2}\int_0^T x^T Q_{\text{VPI(N)}} x + R_{\text{VPI(N)}} u^2 \, dt \tag{64}$$

The diagonal gains of $Q_{\text{VARE}} \in \mathbb{R}^{12\times12}$ have been set empirically, except the already assigned diagonal values of $Q_{\text{VPI(N)}} \in \mathbb{R}^{4\times4}$, and dynamic trends have been identified that could improve the overall system response:

$$Q_{\text{VARE}} = \begin{bmatrix} Q_{\text{VPI(N)}} & 0 \\ 0 & Q_{\text{VARE}_{set_i}} \end{bmatrix} \text{ with } i = 1, 2$$

$$R_{\text{VARE}} = R_{\text{VPI(N)}} \tag{65}$$

Figure 7. Wing dynamic regimes: stable and unstable flight.

Table 4. Numerical simulation parameters.

Scenarios			Control Gains	Values
$U\left[\frac{m}{s}\right]$	$\frac{x_e}{c}$	Initial conditions $[h_0; \dot{h}_0; \alpha_0; \dot{\alpha}_0]\left[m; \frac{m}{s}; \deg; \frac{\deg}{s}\right]$		
11 stable dynamic 13 unstable dynamic	-0.2	$[-0.1; -0.1; -7; 0.05]$	$\boldsymbol{Q}_{\text{VPI}(N)}$	$\text{diag}([100; 100; 0.1; 0.01])$
			$\boldsymbol{Q}_{\text{VARE}}$	$\text{diag}\left(\left[\text{diag}(\boldsymbol{Q}_{\text{VPI}(N)}); \text{diag}(\boldsymbol{Q}_{\text{VARE}_{\text{set}_i}})\right]\right)$
			$\boldsymbol{Q}_{\text{VARE}_{\text{set}_1}}$	$\text{diag}([10; 10; 10; 10; 100; 100; 1; 1] \cdot 10^{-4})$
			$\boldsymbol{Q}_{\text{VARE}_{\text{set}_2}}$	$\text{diag}([1; 1; 1; 1; 100; 100; 0.1; 0.1] \cdot 10^{-4})$
			$R_{\text{VARE}} = R_{\text{VPI}(N)}$	100
9 stable dynamic 10 unstable dynamic	0.1	$[0.1; 0.5; -5; 0.1]$	$\boldsymbol{Q}_{\text{VPI}(N)}$	$\text{diag}([10^6; 10^6; 100; 0.1])$
			$\boldsymbol{Q}_{\text{VARE}}$	$\text{diag}\left(\left[\text{diag}(\boldsymbol{Q}_{\text{VPI}(N)}); \text{diag}(\boldsymbol{Q}_{\text{VARE}_{\text{set}_i}})\right]\right)$
			$\boldsymbol{Q}_{\text{VARE}_{\text{set}_1}}$	$\text{diag}([600; 10; 10; 0.1; 10^{-2}; 10^{-2}; 10^{-4}; 10^{-4}])$
			$\boldsymbol{Q}_{\text{VARE}_{\text{set}_2}}$	$\text{diag}([10; 1; 10; 0.1; 0.1; 0.1; 10^{-2}; 10^{-2}])$
			$R_{\text{VARE}} = R_{\text{VPI}(N)}$	10^6
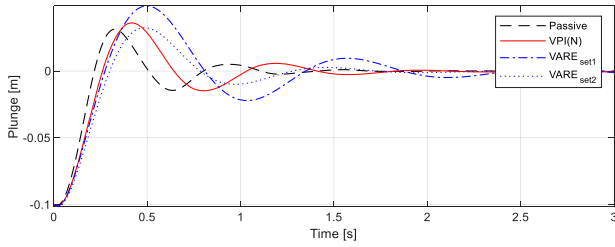
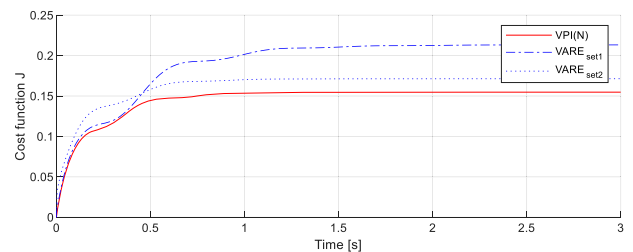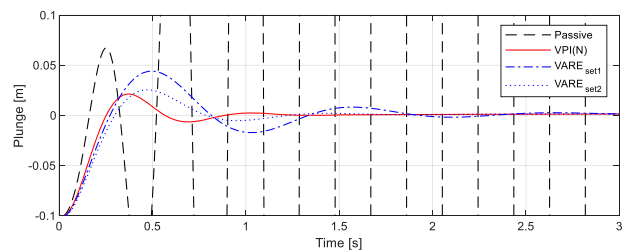**Figure 8.** Plunge time evolution for $U = 11\frac{m}{s}$ and $\frac{x_e}{c} = -0.2$.
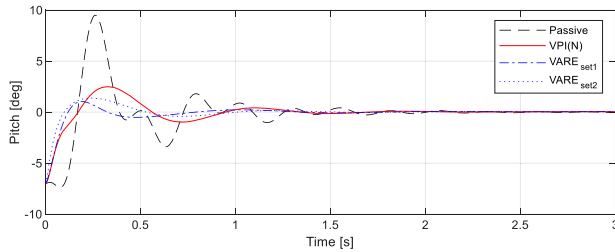
Figure 9. Pitch time evolution for $U = 11\frac{m}{s}$ and $\frac{x_e}{c} = -0.2$.
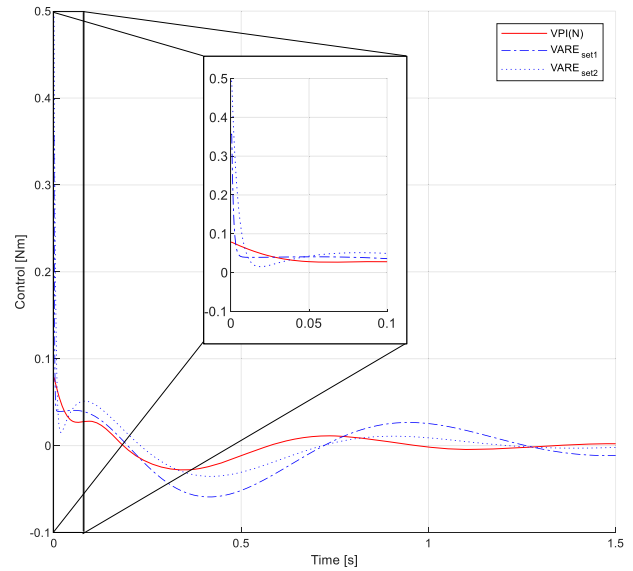
Figure 10. Control action for $U = 11\frac{m}{s}$ and $\frac{x_e}{c} = -0.2$ (with horizontal zoom until 0.1 s).

However, it appears the VARE results are very sensitive to the choice of the gains $\boldsymbol{Q}_{\text{VARE}_{\text{set}_i}} \in \mathbb{R}^{8 \times 8}$, and a more exhaustive search could be performed through parametric optimisation techniques, not the subject of this paper.

Let's consider Figures 8–11 relative to the stable case, with an inflow velocity of $11\frac{m}{s}$ and a characteristic ratio $\frac{x_e}{c} = -0.2$. The VARE and the VPI(N) both control the plunge in the same way, with a better settling time for the VPI(N), and a higher overshoot for the $\text{VARE}_{\text{set}_1}$. The pitch is instead better controlled by the $\text{VARE}_{\text{set}_1}$, with smaller oscillation amplitudes with respect to the VPI(N). The intensity of the control action is similar for all three cases, except for some initial values, for which the VARE requires an intensity of the control of 4–5 times greater than those used by VPI(N). Finally, the cost function J calculated by Equation (64) is lower for the VPI(N).

The same set of the Q_i, R gains is used to test the wing response under conditions of dynamic flutter instability for an inflow speed of $13\frac{m}{s}$ (see Figures 12–15). Obviously, as intuitive, the passive response shows unstable flutter with very large amplitudes, while the active controls both stabilise very effectively the wing motion.

In Figures 16–19, the controls are compared for $\frac{x_e}{c} = 0.1$ and an inflow speed of 9m/s. The plunge is controlled in the same

Figure 11. Cost function time evolution for $U = 11\frac{m}{s}$ and $\frac{x_e}{c} = -0.2$.

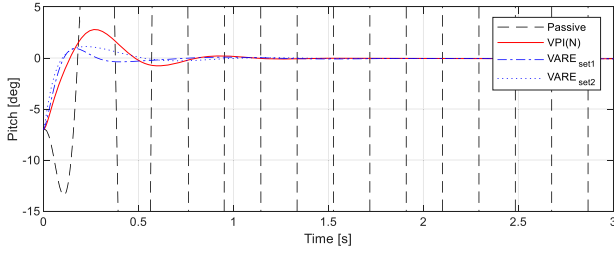**Figure 12.** Plunge time evolution for $U = 13\frac{m}{s}$ and $\frac{x_e}{c} = -0.2$.

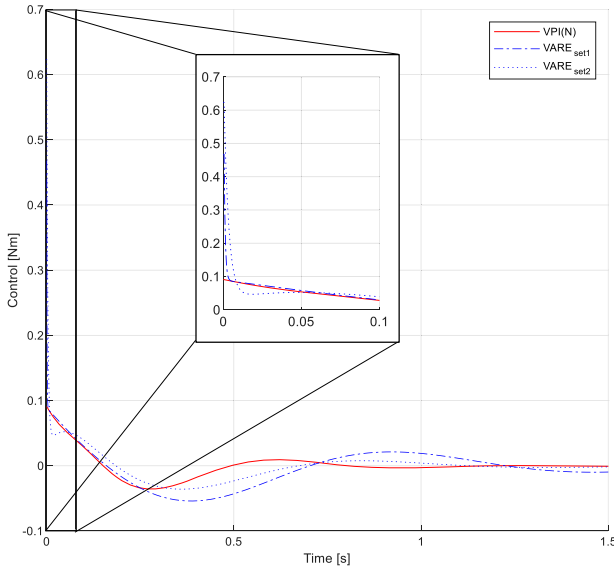**Figure 13.** Pitch time evolution for $U = 13\frac{m}{s}$ and $\frac{x_e}{c} = -0.2$.

Figure 14. Control action for $U = 13\frac{m}{s}$ and $\frac{x_e}{c} = -0.2$ (with horizontal zoom until 0.1s).
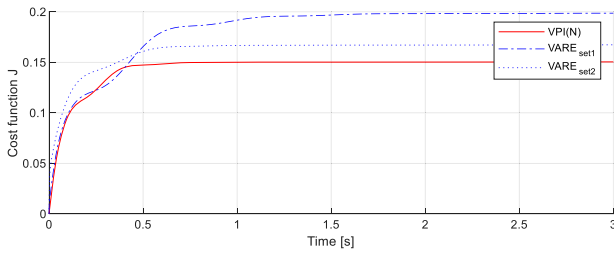

Figure 15. Cost function time evolution for $U = 13\frac{m}{s}$ and $\frac{x_e}{c} = -0.2$.

Figure 16. Plunge time evolution for $U = 9\frac{m}{s}$ and $\frac{x_e}{c} = 0.1$.

Figure 17. Pitch time evolution for $U = 9\frac{m}{s}$ and $\frac{x_e}{c} = 0.1$.

Figure 18. Control action for $U = 9\frac{m}{s}$ and $\frac{x_e}{c} = 0.1$(zoom until 0.6s).

way by all the three controls, with slightly higher oscillations for the VPI(N), which shows the highest settling time. For the pitch, the best control is obtained by the VARE$_{set_2}$ which, however, requires an initial control intensity more than double for the set2 and even three times for the set1.

Finally, in Figures 20–23, a diverging wing instability is investigated, with the same Q_i, R of the previous case, but an increased inflow speed ($U = 10\frac{m}{s}$). The wing response remains almost similar with respect to the previous cases, except for a slight worsening in the cost function of VPI(N).

In conclusion, it appears that both the new controls produce good performances in both stable and unstable aerofoil conditions and that both the methods, VPI(N) and VARE, exhibit performances strongly depending on the selection of the tuning
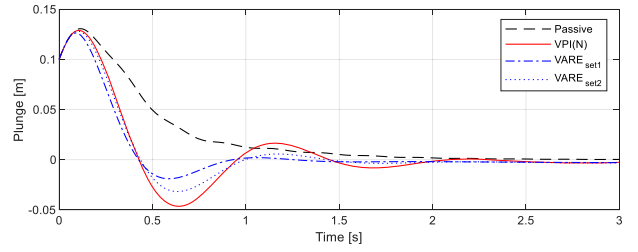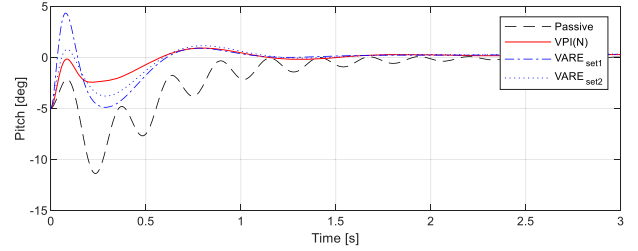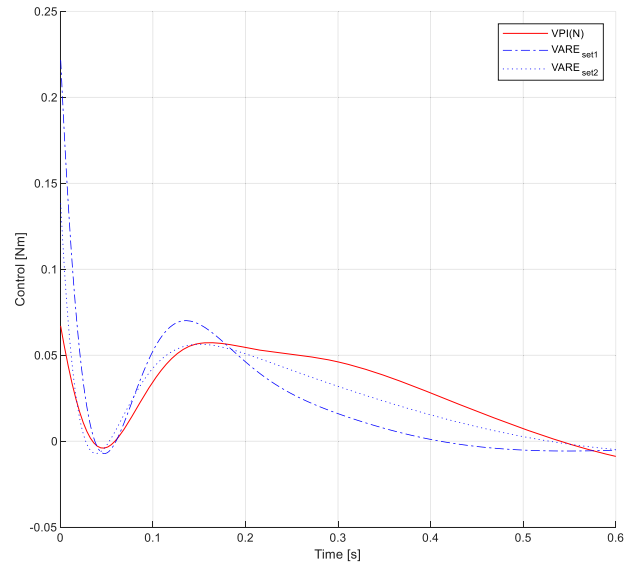
parameters appearing in the matrices **Q** and **R**, not determining a definite ranking between the two. However, we remark the VPI(N) presents a smaller set of tuning parameters Q_i with respect to the VARE, making probably its use simpler.

4.3. Case study of an unsteady blade wind turbine dynamic

In the following paragraph, the control is applied to the blade of a wind turbine in flutter condition. Typically, the wind blades are oriented in angle of attack through rotary motors contained in the ogive (see Figure 24) and this allows to maximise the energy extracted from the wind in all conditions. When the wind speed exceeds a critical threshold, the motors orient the blades to the wind so that they do not generate lifts on the blades
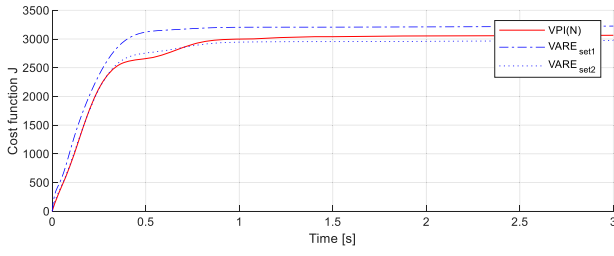
Figure 19. Cost function time evolution for $U = 9\frac{m}{s}$ and $\frac{x_e}{c} = 0.1$.
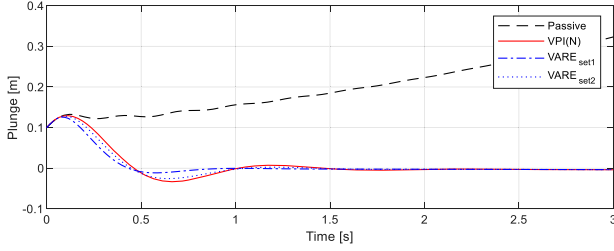

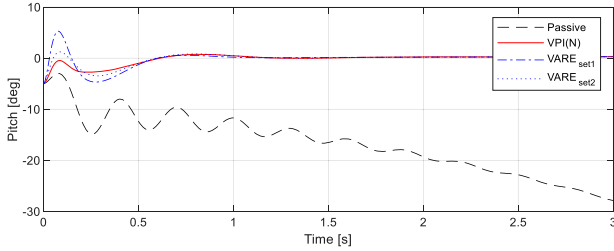**Figure 20.** *Plunge* time evolution for $U = 10\frac{m}{s}$ and $\frac{x_e}{c} = 0.1$.

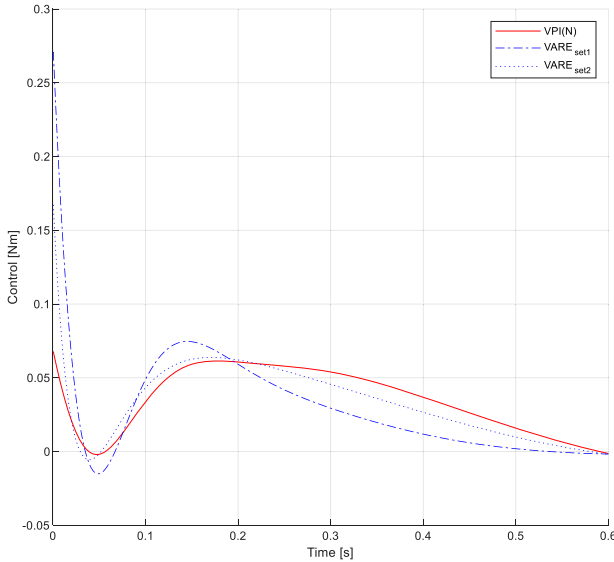**Figure 21.** Pitch time evolution for $U = 10\frac{m}{s}$ and $\frac{x_e}{c} = 0.1$.

Figure 22. Control action for $U = 10\frac{m}{s}$ and $\frac{x_e}{c} = 0.1$ (zoom until 0.6s).

and therefore can stop the rotor. This speed is also called cut-off speed, beyond which the blades are subject to vibration with the risk of generating structural damage due to the high oscillations they can reach. In the present study, a wind turbine is modelled, inspired by a plant of 5MW (Pourazarm et al., 2016;
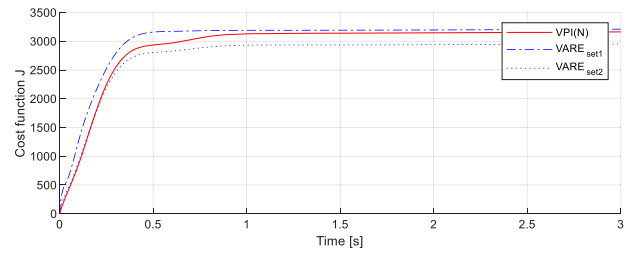

Figure 23. Cost function time evolution for $U = 10\frac{m}{s}$ and $\frac{x_e}{c} = 0.1$.
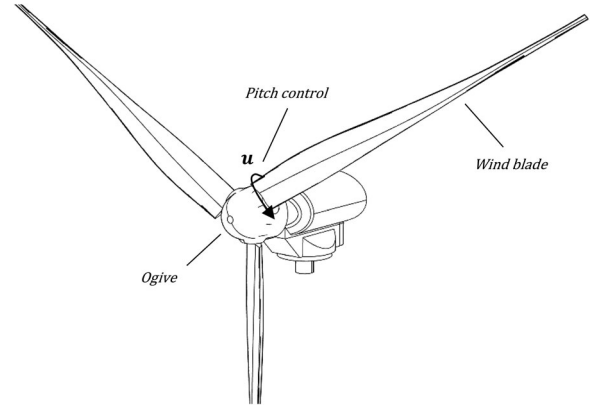

Figure 24. Sketch of wind turbine blades controlled in attack angle.

Shakya et al., 2019) subject to bending and torsional vibrations and is controlled in the unstable conditions of flutter through the orientation of the blade.

The equations of motion characterising the flapwise displacement $w(x, t)$ and the torsional displacement $\varphi(x, t)$ of a wind turbine blade (see Figure 25) are the equations of (Hodges & Dowell, 1974):

$$
\begin{aligned}
&\left[EIw'' - e\varphi \int_x^L \Omega^2 \rho A x dx\right]'' - \left[w' \int_x^L \Omega^2 \rho A x dx\right]' - (\Omega^2 mex\varphi)' \\
&\quad + m(\ddot{w} + e\ddot{\varphi}) = L_C + L_{NC} \\
&\quad - \left[\left(GJ + K_m^2 \int_x^L \Omega^2 \rho A x dx\right)\varphi'\right]' + \Omega^2 \rho A(K_{m2}^2 - K_{m1}^2)\varphi \\
&\quad + \rho A K_m^2 \ddot{\varphi} - \left(\int_x^L \Omega^2 \rho A x dx\right)ew'' + \Omega^2 mxew' + me\ddot{w} \\
&= M_C + M_{NC} + u(t)\delta(x)
\end{aligned}
\tag{66}
$$

where EI and GJ are the bending and torsional stiffness; K_m, K_{m1} and K_{m2} are the gyration radius over x, y, and z axis; m, ρ are the mass per unit length and the blade material density; A is the cross-section area; e is the distance between the elastic axis and the centroid of mass; Ω is the rotor speed; $L_C(t)$, $L_{NC}(t)$ and $M_C(t)$, $M_{NC}(t)$, as described in the previous paragraph, are the lift force and pitching moment acting on the blade, due to the circulatory (C) and the non-circulatory (NC) contributions of the aerodynamic load.

The term $u(t)$, in the second equation, represents the torque control action applied on the blade and is represented by the Dirac distribution.
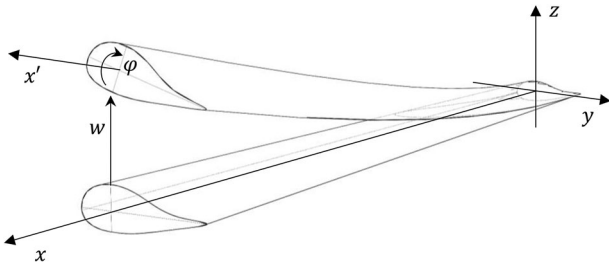
Figure 25. Wind blade with bending and torsional deformation.

including N modes:

$$w(x,t) = \sum_{j=1}^{N} \Psi_{w_j}(x)\varsigma_j(t)$$

$$\varphi(x,t) = \sum_{j=1}^{N} \Psi_{\varphi_j}(x)\theta_j(t) \qquad (67)$$

Equations (46)–(49) are substituted into Equation (66), and $h = -w, \alpha = \varphi$. To solve the coupled partial differential equations, the Galerkin method is used by a modal decomposition

Multiplying its corresponding eigenfunctions and integrating over the beam length, the set of Volterra equations can be obtained:

$$(M_s + M_A)\ddot{q} + C_A\dot{q} + (K_s + K_A)q = F_A * \dot{\phi} + Cu \qquad (68)$$
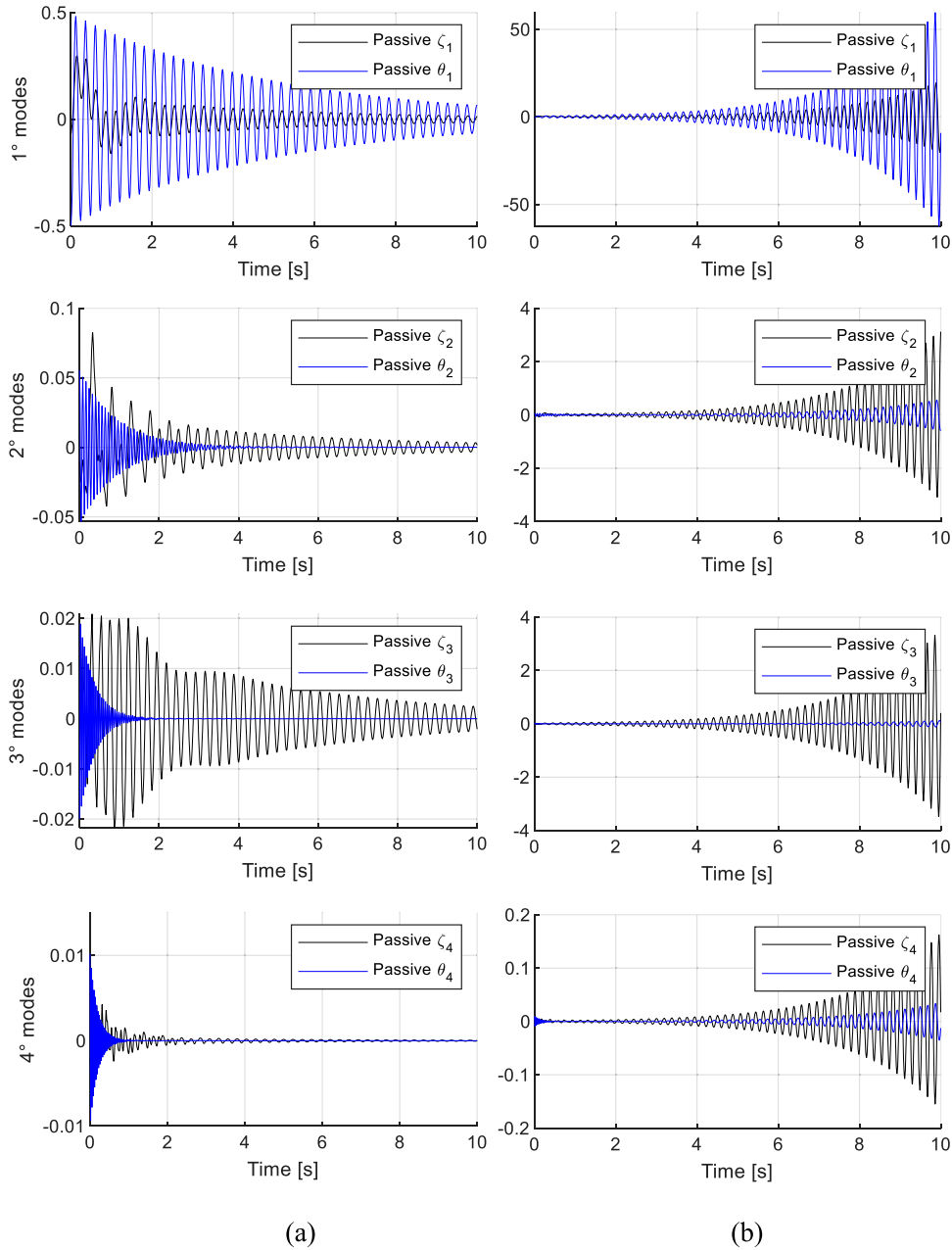

(a)

(b)

Figure 26. Modal coordinates of the uncontrolled wind turbine blade subject to initial conditions other than zero: (a) stable behaviour with nominal omega (b) unstable behaviour with flutter omega.
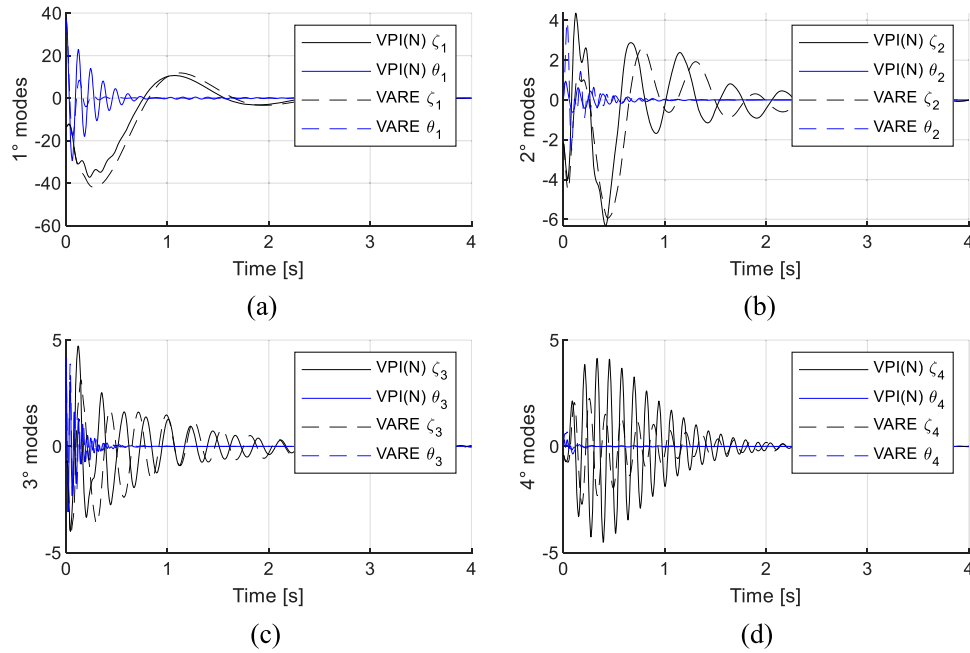
Figure 27. Trend of control laws VPIN and VARE for modal coordinates: (a) first mode (b) second mode (c) third mode and (d) fourth mode.

Table 5. Wind blade parameters.

Parameters		Values				
c	Chord	4				[m]
s	Span	62.6				[m]
f_w	Bending natural frequencies	[0.65	2	4.5	8.2]	[Hz]
f_φ	Torsional natural frequencies	[4	12.1	20.3	28.4]	[Hz]
ρ	Density	721				[kg/m³]
e	Distance between mass centroid and the elastic axis	0.13				[m]
m	Mass per unit length	225.8				[kg/m]
A	Section area	2.75				[m²]
EI	Bending stiffness	$5.5315e + 08$				[Nm²]
GJ	Torsional stiffness	$2.6962e + 09$				[Nm²]
$\Omega; \Omega_f$	Rated rotor Speed; Flutter rotor speed	12.1; 22.1				[RPM]
R_m	Mean radius	31.7				[m]
K_{m1}	Radius of gyraon	0.28				[m]
K_{m2}		0.85				[m].
K_m		0.89				[m]
$[\varepsilon_1; \psi_1; \varepsilon_2; \psi_2]$	Kernel parameters	[0.041; 0.165; 0.32; 0.335]				–

where M_s, K_s are structural matrices, while M_A, K_A, C_A are aerodynamic matrices, with dimension $\mathbb{R}^{2N \times 2N}$, and $F_A \in \mathbb{R}^{2N}$ is an aerodynamic vector associated with the circulation effect, and C is a control vector (see Appendix C for the definition of symbols).

In order to make more realistic simulations, we have been inspired by the 5MW turbine (Jonkman et al., 2009), widely studied in the literature (see Table 5). The blade's parameters have been chosen as a function of the bending and torsional natural frequencies found in (Pourazarm et al., 2016; Shakya et al., 2019), in order to recover the critical flutter velocity of about $\Omega_f = 22.1$ RPM with a flutter frequency of 5.5 Hz. The reference wing section used for the medium radius is the Delft University DU25 airfoil for which opensource data is available.

Simulations in the absence of control are shown in Figure 26(a) with the nominal working conditions for the rated rotor speed of $\Omega = 12.1$RPM, while in Figure 26(b) the instability condition for which the flutter occurs appears. In both cases, the initial conditions imposed are a linear deformation both bending and torsion so at the end of the wing we find a displacement of 1 mm and a section rotation of 0.1 degrees.

On the other hand, the controlled flutter conditions are shown in Figure 27, with a linear distribution for the initial displacement conditions, with the blade tip deflected of 20 cm and rotated of 15°, and linear velocity distribution, with strain rate at the tip about 0.01 m/s and 10 rad/s of tip angular velocity, respectively.

The proposed control algorithms are formulated starting from the integro-differential model of the blade, based on a 4-mode decomposition (4 flexural and 4 torsional). In Figure 27, the blue lines represent the rotational modal coordinates while those in black are the flexural ones.

For the first mode in Figure 27(a) the VPI(N) method shows a very good control of the rotational oscillations just after 1s of simulation. Indirectly, the flexural oscillations are also controlled after 4s, obtaining a strong damping of the oscillations. Instead, VARE control provides the total attenuation even in a shorter time (0.5 s), allowing slightly larger flexural oscillation. The performance of the VARE is obviously paid in terms of power and torque action; in fact, anticipating the attenuation times requires a larger effort of control (Figure 28).

The other 3 modes of response are represented in Figure 27(b–d). For the second mode, VPI(N) control is characterised by smaller oscillations than the others. In the fourth mode, on the other hand, VARE shows a better result.

The cost function, shown in Figure 29, turns out to be better (lower value) for the VPI(N) controller. In general, we conclude that the results largely depend on the tuning parameters of the controllers. It may be possible that a different choice of tuning
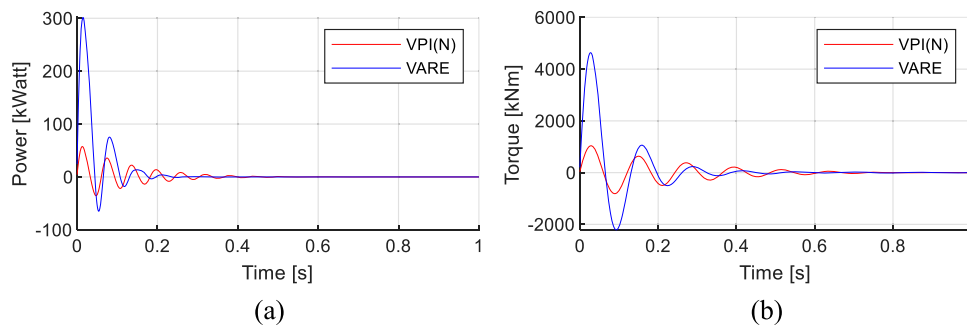
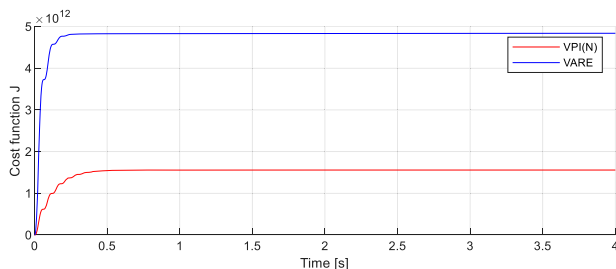**Figure 28.** Power (a) and torque (b) evolution for VPI(N) and VARE.

Figure 29. Cost functions evolution for VPI(N) and VARE.

parameters can change the results and invert the ranking of the performances of the two methods. Both controllers work very well and give the possibility to study different patterns and explore different scenarios.

5. Conclusion

This paper aims to contribute to the optimal control of Volterra IDEs with special application to the flutter control of a wing in a fluid flow.

A common physical background to the appearance of integral and convolutional terms in the equation of engineering interest is outlined, emphasising how these memory effects can be borne in problems in which two different fields are coupled, with emphasis to the problem of fluid-structure interaction, one of the most significant for engineering applications.

Two examples considered in detail in the present paper are that of an airfoil oscillating in a fluid flow, and of a rotating wind turbine blade, looking for optimal control of their unstable flutter oscillation. Since the problem couples the rigid body equations of the structure with that of the flow, where the flow field variables are not explicitly appearing (hidden variables), a mechanism of generation of integral memory terms appears, consistent with the general view provided in the paper.

Two different methods are presented to approach the control of integro-differential equations, both leading to an analytical form of the control u in terms of an integral Volterra equation, that can be readily solved numerically.

The first method, after a direct Laplace transformation of the equations, possible because the exponential expansion of the kernel, determines the Volterra Algebraic Riccati Equation-VARE for the integro-differential problem, while the second introduces an indirect variational method which meets the optimality conditions VPI(N). Both controllers start from an IDE

model in its scalar simplest form, under the hypothesis the kernel has a series exponential form, which is reasonable in many physical problems, as in the case of control of the aerofoil flutter studied in detail.

Although both controllers determine an explicit analytical form of the minimum cost problem, leading to the same Volterra integral equation for the control, they show differences which are emphasised by the numerical results. Differently from VPI(N) method, the optimal control VARE requires a number of additional tuning parameters equal to the number of the exponential terms of the kernel.

Furthermore, both the VARE and the VPI(N) controls guarantee stability and robustness. In fact, in the first method, the stability comes directly from the control gain derived by the steady Riccati's equation through the LQR. For the second method, a suitable selection of the eigenvalues (those with negative real part) and associated eigenvectors makes the solution intrinsically stable, being the modal expansion deprived by the diverging terms.

Both applications of controlled flutter show very good performance.

Future developments will involve the development of a complete model for wind turbines including the study of the actuator's dynamic in order to apply this control theory to a real wind turbine.

Disclosure statement

No potential conflict of interest was reported by the author(s).

ORCID

G. Pepe http://orcid.org/0000-0002-1444-7765

References

Abdel Hafeez, M. M., & El-Badawy, A. A. (2018). Flutter limit investigation for a horizontal axis wind turbine blade. *Journal of Vibration and Acoustics*, 140(4), 12. https://doi.org/10.1115/1.4039402

Ahmad, J., & Mohyud-Din, S. T. (2013). Homotopy analysis method with modified Reimann-Liouville derivative for space fractional diffusion equation. *International Journal of Physical Sciences*, 8(43), 1994–1999. https://doi.org/10.5897/IJPS2013.4014

Al Azzawi, W., Herath, M., & Epaarachchi, J. (2019). 15 - Modeling, analysis, and testing of viscoelastic properties of shape memory polymer composites and a brief review of their space engineering applications. In R. M. Guedes (Ed.), *Creep and fatigue in polymer matrix composites* (2nd ed.) (pp. 465–495). Woodhead Publishing. https://doi.org/10.1016/B978-0-08-102601-4.00015-1

Babaei, B., Velasquez-Mao, A. J., Thomopoulos, S., Elson, E. L., Abramow-itch, S. D., & Genin, G. M. (2017). Discrete quasi-linear viscoelastic damping analysis of connective tissues, and the biomechanics of stretching. *Journal of the Mechanical Behavior of Biomedical Materials*, *69*, 193–202. https://doi.org/10.1016/j.jmbbm.2016.12.013

Belbas, S. A. (2007). A new method for optimal control of Volterra integral equations. *Applied Mathematics and Computation*, *189*(2), 1902–1915. https://doi.org/10.1016/j.amc.2006.12.077

Belbas, S. A. (2008). A reduction method for optimal control of Volterra integral equations. *Applied Mathematics and Computation*, *197*(2), 880–890. https://doi.org/10.1016/j.amc.2007.08.093

Benjamin, M. R., Battle, D., Eickstedt, D., Schmidt, H., & Balasuriya, A. (2007, April). Autonomous Control of an Autonomous Underwater Vehicle Towing a Vector Sensor Array. Proceedings 2007 IEEE International Conference on Robotics and Automation.

Byron, F. W., & Fuller, R. W. (2012). *Mathematics of classical and quantum physics*. Courier Corporation.

Caputo, M., & Fabrizio, M. (2015). A new definition of fractional derivative without singular kernel. *Progress in Fractional Differentiation and Applications*, *1*(2), 1–13. https://www.naturalspublishing.com/files/published/0gb83k287mo759.pdf

Carcaterra, A., & Akay, A. (2011). Dissipation in a finite-size bath [article]. *Physical Review E – Statistical, Nonlinear, and Soft Matter Physics*, *84*(1), 1, Article 011121. https://doi.org/10.1103/PhysRevE.84.011121

Carcaterra, A., Coppo, F., Mezzani, F., & Pensalfini, S. (2019). Long-range retarded elastic metamaterials: Wave-stopping, negative, and hypersonic or superluminal group velocity. *Physical Review Applied*, *11*(1), Article 014041. https://doi.org/10.1103/PhysRevApplied.11.014041

Carcaterra, A., Dessi, D., & Mastroddi, F. (2005). Hydrofoil vibration induced by a random flow: A stochastic perturbation approach. *Journal of Sound and Vibration*, *20*(283), 401–432. https://doi.org/10.1016/j.jsv.2004.04.040

Carcaterra, A., Roveri, N., & Pepe, G. (2015). Fractional dissipation generated by hidden wave-fields. *Mathematics and Mechanics of Solids*, *20*(10), 1251–1262. https://doi.org/10.1177/1081286513518941

Carillo, S. (2017). Regular and singular kernel problems in magneto-viscoelasticity. *Meccanica*, *52*(13), 3053–3060. https://doi.org/10.1007/s11012-017-0722-1

de Andrade, B. (2018). On the well-posedness of a Volterra equation with applications in the Navier-Stokes problem. *Mathematical Methods in the Applied Sciences*, *41*(2), 750–768.

Dehghan, M., & Shakeri, F. (2008). Solution of an integro-differential equation arising in oscillating magnetic fields using He's homotopy perturbation method. *Progress in Electromagnetics Research*, *78*, 361–376. https://doi.org/10.2528/PIER07090403

Hodges, D. H., & Dowell, E. H. (1974). *Nonlinear equations of motion for the elastic bending and torsion of twisted nonuniform rotor blades*.

Jones, R. T. (1940). *The unsteady lift of a wing of finite aspect ratio* (Vol. 681). Naca report.

Jonkman, J., Butterfield, S., Musial, W., & Scott, G. (2009). Definition of a 5-MW reference wind turbine for offshore system development. *National Renewable Energy Laboratory*, https://doi.org/10.2172/947422

Kochetkov, Y. A., & Tomshin, V. K. (1978). Optimal control of deterministic systems described by integro-differential equations. *Avtomatika i Telemekhanika*, *20*(1), 5–11. http://www.mathnet.ru/php/archive.phtml?wshow=paper&jrnid=at&paperid=9613&option_lang=eng

Kumar, S., Onkar, A. K., & Manjuprasad, M. (2020). Stochastic modeling and reliability analysis of wing flutter. *Journal of Aerospace Engineering*, *33*(5), Article 04020044. https://doi.org/10.1061/(ASCE)AS.1943-5525.0001153

Levinson, N. (1960). A nonlinear Volterra equation arising in the theory of superfluidity. *Journal of Mathematical Analysis and Applications*, *1*(1), 1–11. https://doi.org/10.1016/0022-247X(60)90028-7

Maleknejad, K., & Almasieh, H. (2011). Optimal control of Volterra integral equations via triangular functions. *Mathematical and Computer Modelling*, *53*(9-10), 1902–1909. https://doi.org/10.1016/j.mcm.2011.01.017

Maleknejad, K., & Ebrahimzadeh, A. (2014). Optimal control of Volterra integro-differential collocation method.

Marzban, H. R., & Rostami Ashani, M. (2020). A class of nonlinear optimal control problems governed by Fredholm integro-differential

equations with delay. *International Journal of Control*, *93*(9), 2199–2211. https://doi.org/10.1080/00207179.2018.1550683

Mo, W., Li, D., Wang, X., & Zhong, C. (2015). Aeroelastic coupling analysis of the flexible blade of a wind turbine. *Energy*, *89*, 1001–1009. https://doi.org/10.1016/j.energy.2015.06.046

Mohammad Naser, M. F., & Ikhouane, F. (2015). Hysteresis loop of the LuGre model. *Automatica*, *59*, 48–53. https://doi.org/10.1016/j.automatica.2015.06.006

Newman, J. N. (1979). The theory of ship motions. In J. N. Newman (Ed.), *Advances in applied mechanics* (Vol. 18, pp. 221–283). Elsevier. https://doi.org/10.1016/S0065-2156(08)70268-0

Nutting, P. G. (1921). A study of elastic viscous deformation. *Proceedings – American Society for Testing and Materials*, *21*, 1162–1171.

Olsen, W., & Wagner, J. (1982). Effect of thickness on airfoil surface noise. *AIAA Journal*, *20*(3), 437–439. https://doi.org/10.2514/3.7922

Paifelman, E. (2017). A comparison between mathematical models of stationary configuration of an underwater towed system with experimental validations for oceans'17 MTS/IEEE Aberdeen conferences. OCEANS 2017 – Aberdeen.

Paifelman, E., Pepe, G., & Carcaterra, A. (2019, 25–28 June 2019). Optimal control with memory effects: theory and application to wings. 2019 18th European Control Conference (ECC).

Paifelman, E., Pepe, G., & Carcaterra, A. (2021). An optimal indirect control of underwater vehicle. *International Journal of Control*, *94*(2), 312–326. https://doi.org/10.1080/00207179.2019.1590737

Paifelman, E., Pepe, G., La Gala, F., & Carcaterra, A. (2018). Control of fluctuations of a tethered unmanned-underwater-vehicle. Proceedings of ISMA 2018 – International Conference on Noise and Vibration Engineering and USD 2018 - International Conference on Uncertainty in Structural Dynamics.

Pepe, G., & Carcaterra, A. (2014). Semi-active damping by variational control algorithms. Proceedings of the International Conference on Structural Dynamic, EURODYN.

Pepe, G., Mezzani, F., Carcaterra, A., Cedola, L., & Rispoli, F. (2020). Variational control approach to energy extraction from a fluid flow. *Energies*, *13*(18), 18, Article 4913. https://doi.org/10.3390/en13184913.

Pepe, G., Paifelman, E., & Carcaterra, A. (2020a). Optimal feedback control law for viscoelastic materials with memory effects. Proceedings of the International Conference on Structural Dynamic, EURODYN2020, Athens, Greece.

Pepe, G., Paifelman, E., & Carcaterra, A. (2020b). Volterra models of magnetorheological dampers and their application to vibrating systems. Proceedings of ISMA 2020 – International Conference on Noise and Vibration Engineering and USD 2020 – International Conference on Uncertainty in Structural Dynamics.

Pepe, G., Paifelman, E., & Carcaterra, A. (2021). *Aeroelastic dynamic feedback control of a Volterra's airfoil*. Nonlinear Dynamics Conference NODYCON 2021, Rome.

Pontryagin, L. S. (2018). *Mathematical theory of optimal processes*. Routledge.

Pourazarm, P., Modarres-Sadeghi, Y., & Lackner, M. (2016). A parametric study of coupled-mode flutter for MW-size wind turbine blades. *Wind Energy*, *19*(3), 497–514. https://doi.org/10.1002/we.1847

Rao, L. G., & Allison, J. T. (2015, August). Generalized viscoelastic material design with integro-differential equations and direct optimal control. Volume 2B: 41st Design Automation Conference.

Rezaei, A. S., Mezzani, F., & Carcaterra, A. (2019). Memory effects in wave propagation. Proceedings of the 26th International Congress on Sound and Vibration, ICSV 2019.

Roberts, J. D. (1980). Linear model reduction and solution of the algebraic Riccati equation by use of the sign function. *International Journal of Control*, *32*(4), 677–687. https://doi.org/10.1080/00207178008922881

Sachs, E. W., & Strauss, A. K. (2008). Efficient solution of a partial integro-differential equation in finance. *Applied Numerical Mathematics*, *58*(11), 1687–1703. https://doi.org/10.1016/j.apnum.2007.11.002

Shakya, P., Sunny, M. R., & Maiti, D. K. (2019). A parametric study of flutter behavior of a composite wind turbine blade with bend-twist coupling. *Composite Structures*, *207*, 764–775. https://doi.org/10.1016/j.compstruct.2018.09.064

Singha, N., & Nahak, C. (2018). A numerical method for solving a class of fractional optimal control problems using Boubaker polynomial expansion scheme. *Filomat*, 32(13), 4485–4502. https://doi.org/10.2298/FIL1813485S

Solodusha, S. V. (2020). New Classes of Volterra Integral Equations of the First Kind Related to the Modeling of the Wind Turbine Dynamics. Proceedings of 2020 15th International Conference on Stability and Oscillations of Nonlinear Control Systems (Pyatnitskiy's Conference), STAB 2020.

Tao, Q., & Gao, H. (2020). On the null controllability of parabolic equations with nonlinear memory. *International Journal of Control*, 93(7), 1745–1753. https://doi.org/10.1080/00207179.2018.1531148

Theodorsen, T. (1933). Theory of wing sections of arbitrary shape.

Tohidi, E., & Samadi, O. R. N. (2013). Optimal control of nonlinear Volterra integral equations via Legendre polynomials. *IMA Journal of Mathematical Control and Information*, 30(1), 67–83. https://doi.org/10.1093/imamci/dns014

Vasconcellos, R. M. G. d., Pereira, D. d. A., & Marques, F. D. (2016). Characterization of nonlinear behavior of an airfoil under stall-induced pitching oscillations. *Journal of Sound and Vibration*, 372, 283–298. https://doi.org/10.1016/j.jsv.2016.02.046

Vijayakumar, V. (2018). Approximate controllability results for analytic resolvent integro-differential inclusions in Hilbert spaces. *International Journal of Control*, 91(1), 204–214. https://doi.org/10.1080/00207179.2016.1276633

Vinokurov, V. R. (1969). Optimal control of processes described by integral equations. I. *SIAM Journal on Control*, 7(2), 324–336. https://doi.org/10.1137/0307022

Wolf, C., Merz, C., Richter, K., & Raffel, M. (2015). Tip Vortex Dynamics of a Pitching Rotor Blade Tip Model.

Yan, Z., & Lu, F. (2016). The optimal control of a new class of impulsive stochastic neutral evolution integro-differential equations with infinite delay. *International Journal of Control*, 89(8), 1592–1612. https://doi.org/10.1080/00207179.2016.1140229

Yang, Y., & Strganac, T. W. (2013). Experiments of vortex-induced torsional oscillation of a flat plate in cross flow. *AIAA Journal*, 51(6), 1522–1526. https://doi.org/10.2514/1.J051976

Yousefi, S. A., Lotfi, A., & Dehghan, M. (2011). The use of a Legendre multiwavelet collocation method for solving the fractional optimal control problems. *Journal of Vibration and Control*, 17(13), 2059–2065. https://doi.org/10.1177/1077546311399950

Zhou, X. Q., Yu, D. Y., Shao, X. Y., Zhang, S. Q., & Wang, S. (2016). Research and applications of viscoelastic vibration damping materials: A review. *Composite Structures*, 136, 460–480. https://doi.org/10.1016/j.compstruct.2015.10.014

Appendices

Appendix A

Below is the generalisation of the result presented in Section 3.1 considering an exponential series of the kernel:

$$k(t) = \sum_{k=1}^{N} \alpha_k e^{-\beta_k t} \tag{69}$$

where its Laplace transformation can be expressed as a ratio of a series of polynomials of combinations of the coefficients α_k and β_k:

$$\mathcal{L}\{k * x\} = X(s)\frac{P^{(N-1)}(s)}{D^{(N)}(s)} \tag{70}$$

which can be conveniently grouped with coefficients d_i and p_i:

$$D^{(N)}(s) = s^N + \sum_{i=0}^{N-1} d_i s^i$$

$$P^{(N-1)}(s) = \sum_{i=0}^{N-1} p_i s^i \tag{71}$$

Starting from the Volterra integro-differential equation:

$$\dot{x} = ax + k * x + bu \tag{72}$$

and proceeding with the Laplace transform we obtain:

$$(sX(s) - x_0)D^{(N)}(s) = aD^{(N)}(s)X(s) + P^{(N-1)}(s)X(s) + bD^{(N)}(s)U(s) \tag{73}$$

Now, multiplying Equation (73) by $\frac{1}{s^N}$ and using $\frac{1}{s^N}\sum_{i=0}^{N-1} d_i s^i = \sum_{i=-N}^{-1} d_{N+i}s^i$, we obtain:

$$(sX(s) - x_0) = aX(s) + bU(s) + a\left(\sum_{i=-N}^{-1} d_{N+i}s^i\right)X(s)$$

$$+ \sum_{i=-N}^{-1} p_{N+i}s^i X(s) + b\left(\sum_{i=-N}^{-1} d_{N+i}s^i\right)U(s)$$

$$- (sX(s) - x_0)\sum_{i=-N}^{-1} d_{N+i}s^i \tag{74}$$

Assuming $d_i = 0$ for $i < 0$, than we have:

$$Z_j(s) = (ad_{N-j}X(s) + p_{N-j}X(s) + bd_{N-j}U(s) + x_0 d_{N-j}$$

$$- d_{N-1-j}X(s))s^{-j}\text{with } j = [1,\ldots,N] \tag{75}$$

and Equation (74) becomes:

$$(sX(s) - x_0) = (a - d_{N-1})X(s) + \sum_{j=1}^{N} Z_j(s) + bU(s) \tag{76}$$

Transforming back to time domain, and reducing to first order derivative, we have:

$$\begin{cases} \dot{\tilde{q}}_1 = (a - d_{N-1})\tilde{q}_1 + \tilde{q}_2 + bu \\ \vdots \\ \dot{\tilde{q}}_k = \frac{d^{(k-1)}}{dt^{(k-1)}}\mathcal{L}^{-1}\{Z_{k-1}(s)\} + \tilde{q}_{k+1} \quad \text{with } k = [2,\ldots,N+1] \\ \vdots \end{cases} \tag{77}$$

with $\tilde{q}_k = \frac{d^{(k-2)}}{dt^{(k-2)}}\sum_{j=k-1}^{N}\mathcal{L}^{-1}\{Z_j(s)\}$ and $\mathcal{L}^{-1}\{x_0 d_{N-j}s^{-j}\} = x_0 d_{N-j}\frac{t^{j-1}}{(j-1)!}$ and $\tilde{q}_{N+2} = 0$.

Finally, Equation (77) can be reduced to an LTI system with the state vector $\tilde{q} = [\tilde{q}_1,\ldots,\tilde{q}_{N+1}]$, the matrix $A \in \mathbb{R}^{N+1 \times N+1}$ and $B \in \mathbb{R}^{N+1\ 1}$ and assigned initial conditions $\tilde{q}_0$:

$$\dot{\tilde{q}} = A\tilde{q} + Bu$$

$$i.c.\tilde{q}_0 \tag{78}$$

The optimal control solution can be easily found through the application of the Linear Quadratic Regulator which minimise the quadratic cost function:

$$J = \frac{1}{2}\int_0^T \tilde{q}^T Q\tilde{q} + u^2 R \tag{79}$$

that require $\delta J(\tilde{q}, u) = 0$. The explicit control solution can be obtained through the classic Algebraic Riccati Equations (Roberts, 1980) with its associated gain matrix K:

$$u = -K\tilde{q} \tag{80}$$

Finally, expanding the (80) the final control shows integrals in function of x and u variable:

$$u = -k_1 x + \sum_{i=1}^{N} k_{i+1}\underbrace{\int\ldots\int}_{i}(\hat{d}_i x + \hat{p}_i u)\underbrace{dt\ldots dt}_{i} + \sum_{i=1}^{N} x_0 d_{N-i}\frac{t^{i-1}}{(j-1)!} \tag{81}$$

where $\hat{d}_i$ and $\hat{p}_i$ are groupings of coefficients. The last term depends on the initial state x_0 making the control a non-autonomous function of $N-1$

order. Equation (81) has the following structure:

$$u = f\left(x, \smallint x, \smallint u, \ldots, \underbrace{\smallint \ldots \smallint x}_{i} \underbrace{dt \ldots dt}_{i}, \underbrace{\smallint \ldots \smallint}_{i}\right.$$

$$\left. \times u \underbrace{dt \ldots dt}_{i}, \ldots, t, \ldots, t^{i-1}, \ldots, x_0\right) \tag{82}$$

Note that the same typology of solution is also obtained in the case of the vector Equation (72).

Appendix B

We generalise the theory presented in Section 3.2 (right branch of Figure 3) for N-order series of the exponential kernel (69). Starting from the Laplace transform of (17), we obtain:

$$sX(s) - x_0 = aX(s) + \frac{b^2}{r}\Lambda(s) + \frac{P^{(N-1)}(s)}{D^{(N)}(s)}X(s)$$

$$s\Lambda(s) - \lambda_0 = qX(s) - a\Lambda(s) - \frac{P^{(N-1)}(-s)}{D^{(N)}(-s)}\Lambda(s) \tag{83}$$

where:

$$\mathcal{L}\left\{\smallint_0^\infty k(t-\tau)x(\tau)d\tau\right\} = \sum_i \frac{\alpha_i}{s+\beta_i}X(s) = \frac{P^{(N-1)}(s)}{D^{(N)}(s)}X(s)$$

$$\mathcal{L}\left\{\smallint_0^\infty k(\tau-t)\lambda(\tau)d\tau\right\} = \sum_i \frac{\alpha_i}{s-\beta_i}\Lambda(s) = \frac{P^{(N-1)}(-s)}{D^{(N)}(-s)}\Lambda(s) \tag{84}$$

The $P^{(N-1)}$ and $D^{(N)}$ are polynomials of order $N-1$ and N, respectively, defined as:

$$D^{(N)}(s) = s^N + \sum_{i=0}^{N-1} d_i s^i; D^{(N)}(-s) = s^N + \sum_{i=0}^{N-1} \tilde{d}_i s^i$$

$$P^{(N-1)}(s) = \sum_{i=0}^{N-1} p_i s^i; P^{(N-1)}(-s) = \sum_{i=0}^{N-1} \tilde{p}_i s^i \tag{85}$$

where $d_i, \tilde{d}_i, p_i, \tilde{p}_i$ are suitable coefficients. Dividing Equation (85) by s^N, the equations can be arranged as follow, considering the relation $\frac{1}{s^N}\sum_{i=0}^{N-1} d_i s^i = \sum_{i=-N}^{-1} d_{N+i}s^i$:

$$(sX(s) - x_0) = aX(s) + \frac{b^2}{r}\Lambda(s) + a\left(\sum_{i=-N}^{-1} d_{N+i}s^i\right)X(s)$$

$$+ \frac{b^2}{r}\left(\sum_{i=-N}^{-1} d_{N+i}s^i\right)\Lambda(s) + \sum_{i=-N}^{-1} p_{N+i}s^i X(s)$$

$$- (sX(s) - x_0)\sum_{i=-N}^{-1} d_{N+i}s^i$$

$$(s\Lambda(s) - \lambda_0) = qX(s) - a\Lambda(s) + q\left(\sum_{i=-N}^{-1} \tilde{d}_{N+i}s^i\right)X(s)$$

$$- a\left(\sum_{i=-N}^{-1} \tilde{d}_{N+i}s^i\right)\Lambda(s) + \sum_{i=-N}^{-1} \tilde{p}_{N+i}s^i\Lambda(s)$$

$$- (s\Lambda(s) - \lambda_0)\sum_{i=-N}^{-1} \tilde{d}_{N+i}s^i \tag{86}$$

The d and $\tilde{d}$ coefficients with negative subscript i are null and it is possible to proceed with the following grouping:

$$Z_j(s) = \left(ad_{N-j}X(s) + p_{N-j}X(s) + \frac{b^2}{r}d_{N-j}\Lambda(s)\right.$$

$$\left. + x_0 d_{N-j} - d_{N-1-j}X(s)\right)s^{-j} \text{ with } J = [1, \ldots, N]$$

$$Y_j(s) = (qd_{N-j}X(s) + \tilde{p}_{N-j}\Lambda(s) - a\tilde{d}_{N-j}\Lambda(s)$$

$$+ \lambda_0\tilde{d}_{N-j} - \tilde{d}_{N-1-j}\Lambda(s))s^{-j} \tag{87}$$

this way, Equation (86) is written as:

$$(sX(s) - x_0) = (a - d_{N-1})X(s) + \sum_{j=1}^N Z_j(s) + \frac{b^2}{r}\Lambda(s)$$

$$(s\Lambda(s) - \lambda_0) = -(a + \tilde{d}_{N-1})\Lambda(s) + \sum_{j=1}^N Y_j(s) + qX(s) \tag{88}$$

Laplace anti transform $\mathcal{L}^{-1}\{\}$ and use of the variables $\xi_1 = \mathcal{L}^{-1}\{X(s)\}$, $\eta_1 = \mathcal{L}^{-1}\{\Lambda(s)\}$, $\dot{\xi}_1 = \mathcal{L}^{-1}\{sX(s) - x_0\}$., $\dot{\eta}_1 = \mathcal{L}^{-1}\{s\Lambda(s) - \lambda_0\}$, permits to rewrite Equation (88) as:

$$\begin{cases} \dot{\xi}_1 = (a - d_{N-1})\xi_1 + \xi_2 + \frac{b^2}{r}\eta_1 \\ \quad\vdots \\ \dot{\xi}_k = \frac{d^{(k-1)}}{dt^{(k-1)}}\mathcal{L}^{-1}\{Z_{k-1}(s)\} + \xi_{k+1} \\ \quad\vdots \\ \dot{\eta}_1 = -(a + \tilde{d}_{N-1})\eta_1 + \eta_2 + q\xi_1 \\ \quad\vdots \\ \dot{\eta}_k = \frac{d^{(k-1)}}{dt^{(k-1)}}\mathcal{L}^{-1}\{Y_{k-1}(s)\} + \eta_{k+1} \\ \quad\vdots \end{cases} \text{ with } k = [2, \ldots, N+1] \tag{89}$$

With $\xi_k = \frac{d^{(k-2)}}{dt^{(k-2)}}\sum_{j=k-1}^N \mathcal{L}^{-1}\{Z_j(s)\}$, $\eta_k = \frac{d^{(k-2)}}{dt^{(k-2)}}\sum_{j=k-1}^N \mathcal{L}^{-1}\{Y_j(s)\}$, noting that $\mathcal{L}^{-1}\{x_0 d_{N-j}s^{-j}\} = x_0 d_{N-j}\frac{t^{j-1}}{(j-1)!}$, $\mathcal{L}^{-1}\{\lambda_0\tilde{d}_{N-j}s^{-j}\} = \lambda_0\tilde{d}_{N-j}\frac{t^{j-1}}{(j-1)!}$ and $\xi_{N+2} = \eta_{N+2} = 0$.

Finally, Equation (89) can be reduced to a linear time-invariant system with the state vector $\boldsymbol{v} = [\boldsymbol{\xi}, \boldsymbol{\eta}]^T$, $\boldsymbol{\xi} = [\xi_1, \ldots, \xi_{N+1}]^T$, $\boldsymbol{\eta} = [\eta_1, \ldots, \eta_{N+1}]^T$ and matrix $\boldsymbol{H} = [\boldsymbol{H}_{\xi\xi}\boldsymbol{H}_{\xi\eta}; \boldsymbol{H}_{\eta\xi}\boldsymbol{H}_{\eta\eta}] \in \mathbb{R}^{(2N+2) \times (2N+2)}$ analogously to expression (28).

Consequently, following the same solution methodology illustrated in the previous section, from (28) to (41), it is possible to obtain the infinite-horizon problem solution, i.e. finding the coefficients of the $\boldsymbol{P}$ Riccati's matrix in (27). In this way an analytic expression of the control law can be identified as:

$$u = \frac{b}{r}\left[P_{1,1}x + \sum_{i=1}^N P_{1,i+1}\underbrace{\smallint \ldots \smallint}_{i}(\hat{d}_i x + \hat{p}_i u)\underbrace{dt \ldots dt}_{i}\right.$$

$$\left. + \sum_{i=1}^N x_0 d_{N-i}\frac{t^{i-1}}{(i-1)!}\right] \tag{90}$$

where $[P_{1,1}, \ldots, P_{1,N+1}]$ are the first row elements of the $\boldsymbol{P}$ matrix and $\hat{d}_i$ and $\hat{p}_i$ are suitable constant coefficients. The control presents a combination of integral terms of the same order of the kernel function of the series $k(t)$.

Appendix C

The single matrices which characterise the final equation of motion (68) of the wind turbine's blade are the follows:

$$K_{sj} \begin{bmatrix} EI\Psi_{w_i}\Psi_{w_j}{}^{IV} - \Omega^2\rho A\left[\frac{1}{2}(L^2-x^2)\Psi_{w_i}\Psi_{w_j}{}'' - x\Psi_{w_i}\Psi_{w_j}{}'\right] \\ -e\Omega^2\rho A\Psi_{w_i}\left[\frac{1}{2}(L^2-x^2)\Psi_{\varphi_j}{}'' - 2x\Psi_{\varphi_j}{}' - \Psi_{\varphi_j}\right] \\ -me\Omega^2 x\Psi_{w_i}\Psi_{\varphi_j}{}' - me\Omega^2\Psi_{w_i}\Psi_{\varphi_j} \\ -e\Omega^2\rho A\frac{1}{2}(L^2-x^2)\Psi_{\varphi_i}\Psi_{w_j}{}'' + \Omega^2 mxe\Psi_{\varphi_i}\Psi_{w_j}{}' - GJ\Psi_{\varphi_i}\Psi_{\varphi_j}{}'' \\ -K_m^2\Omega^2\rho A\left[\frac{1}{2}(L^2-x^2)\Psi_{\varphi_i}\Psi_{\varphi_j}{}'' - x\Psi_{\varphi_i}\Psi_{\varphi_j}{}'\right] \\ +\Omega^2\rho A(K_{m2}^2 - K_{m1}^2)\Psi_{\varphi_i}\Psi_{\varphi j} \end{bmatrix}$$

$$M_{A_{ij}} = \begin{bmatrix} \pi\rho b^2\Psi_{w_i}\Psi_{w_j} & \pi\rho b^2 x_e\Psi_{w_i}\Psi_{\varphi_j} \\ \pi\rho b^2 x_e\Psi_{\varphi_i}\Psi_{w_j} & \pi\rho b^4\left(\frac{1}{8} + \frac{x_e^2}{b^2}\right)\Psi_{\varphi_i}\Psi_{\varphi_j} \end{bmatrix}$$

$$K_{A_{ij}} = \begin{bmatrix} 0 & -2\pi\rho U^2 b\phi(0)\Psi_{w_i}\Psi_{\varphi_j} \\ 0 & -2\pi\rho U^2 b^2\left[\frac{1}{2} + \frac{x_e}{b}\right]\phi(0)\Psi_{\varphi_i}\Psi_{\varphi_j} \end{bmatrix}$$

$$C_{A_{ij}} = \begin{bmatrix} 2\pi\rho Ub\phi(0)\Psi_{w_i}\Psi_{w_j} \\ 2\pi\rho Ub^2\left[\frac{1}{2} + \frac{x_e}{b}\right]\phi(0)\Psi_{\varphi_i}\Psi_{w_j} \end{bmatrix}$$

$$\times \begin{bmatrix} -2\pi\rho Ub^2\left(\frac{1}{2} - \frac{x_e}{b}\right)\phi(0)\Psi_{w_i}\Psi_{\varphi_j} - \pi\rho Ub^2\Psi_{w_i}\Psi_{\varphi_j} \\ \pi\rho Ub^3\left(\frac{1}{2} - \frac{x_e}{b}\right)\left(1 - \left[1 + \frac{2x_e}{b}\right]\phi(0)\right)\Psi_{\varphi_i}\Psi_{\varphi_j} \end{bmatrix}$$

$$F_{A_i} * \dot{\phi} = \begin{bmatrix} 2\pi\rho Ub\Psi_{w_i}\int_0^t\sum_j\left(U\Psi_{\varphi_j}\theta(\tau) - \Psi_{w_j}\dot{\varsigma}(\tau)\right) \\ + \Psi_{\varphi_j}\dot{\theta}(\tau)\left(\frac{1}{2} - \frac{x_e}{b}\right)b\right)\dot{\phi}(t-\tau)d\tau \\ 2\pi\rho Ub^2\left[\frac{1}{2} + \frac{x_e}{b}\right]\Psi_{\varphi_i}\int_0^t\sum_j\left(U\Psi_{\varphi_j}\theta(\tau) - \Psi_{w_j}\dot{\varsigma}(\tau)\right) \\ + \Psi_{\varphi_j}\dot{\theta}(\tau)\left(\frac{1}{2} - \frac{x_e}{b}\right)b\right)\dot{\phi}(t-\tau)d\tau \end{bmatrix} \quad (91)$$

For all the matrices we can synthetically report the example for M_s while for convolution we have a vector integral:

$$M_s = \int_0^L \begin{bmatrix} M_{s11} & \cdots & M_{s1N} \\ \vdots & \ddots & \vdots \\ M_{sN1} & \cdots & M_{sNN} \end{bmatrix} dx \quad F_A * \dot{\phi} = \left(\int_0^L \begin{bmatrix} F_{A1} \\ \vdots \\ F_{AN} \end{bmatrix} dx\right)$$

$$* \dot{\phi} C = \begin{bmatrix} 0 \\ \Psi_{\varphi_1}(0) \\ \vdots \\ 0 \\ \Psi_{\varphi_N}(0) \end{bmatrix} \quad (92)$$